Cell Reports

Sugar-responsive inhibition of Myc-dependent ribosome biogenesis by Clockwork orange

Graphical abstract

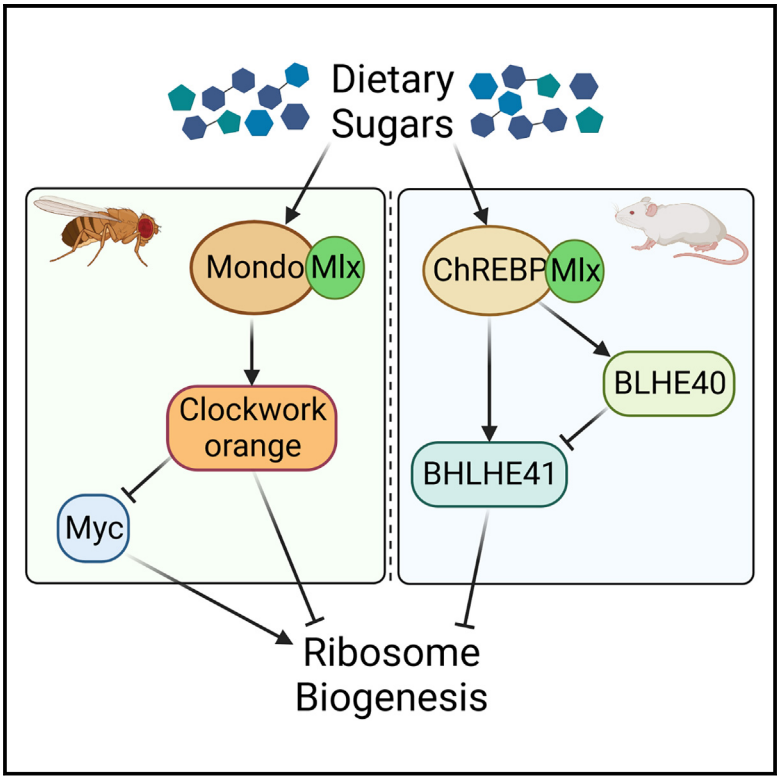

Authors

Linda van den Berg, Krista Kokki, Sylvia J. Wowro, ..., Anni I. Nieminen, Michael Schupp, Ville Hietakangas

Correspondence

ville.hietakangas@helsinki.fi

In brief

van den Berg et al. show that sugar feeding affects several gene expression programs with distinct response kinetics in *Drosophila* larvae, including transient repression of ribosome biogenesis genes. This is mediated by sugar-responsive activation of transcriptional repressor Clockwork orange (CWO), which counteracts Myc, a known activator of ribosome biogenesis.

Highlights

- Sugar feeding regulates kinetically distinct gene expression programs in larvae
- Dietary sugar transiently downregulates ribosome biogenesis gene expression
- CWO and its mouse ortholog BHLHE41 repress ribosome biogenesis genes
- CWO inhibits ribosome biogenesis by counteracting Myc expression and activity

van den Berg et al., 2023, Cell Reports *42*, 112739
July 25, 2023
https://doi.org/10.1016/j.celrep.2023.112739

Cell Reports

CellPress
OPEN ACCESS

Report

Sugar-responsive inhibition of Myc-dependent ribosome biogenesis by Clockwork orange

Linda van den Berg,[1,2] Krista Kokki,[1,2] Sylvia J. Wowro,[3] Konstantin M. Petricek,[3] Onur Deniz,[1,2] Catrin A. Stegmann,[3] Marius Robciuc,[1,2] Mari Teesalu,[1,2] Richard G. Melvin,[4] Anni I. Nieminen,[1,2] Michael Schupp,[3] and Ville Hietakangas[1,2,5,*]

[1]Faculty of Biological and Environmental Sciences, University of Helsinki, 00790 Helsinki, Finland
[2]Institute of Biotechnology, Helsinki Institute of Life Science, University of Helsinki, 00790 Helsinki, Finland
[3]Charité – Universitätsmedizin Berlin, Corporate Member of Freie Universität Berlin and Humboldt-Universität zu Berlin, Institute of Pharmacology, Max Rubner Center (MRC) for Cardiovascular Metabolic Renal Research, 10117 Berlin, Germany
[4]School of Agriculture, Biomedicine and Environment, La Trobe University, Melbourne, VIC 3083, Australia
[5]Lead contact
*Correspondence: ville.hietakangas@helsinki.fi
https://doi.org/10.1016/j.celrep.2023.112739

SUMMARY

The ability to feed on a sugar-containing diet depends on a gene regulatory network controlled by the intracellular sugar sensor Mondo/ChREBP-Mlx, which remains insufficiently characterized. Here, we present a genome-wide temporal clustering of sugar-responsive gene expression in *Drosophila* larvae. We identify gene expression programs responding to sugar feeding, including downregulation of ribosome biogenesis genes, known targets of Myc. Clockwork orange (CWO), a component of the circadian clock, is found to be a mediator of this repressive response and to be necessary for survival on a high-sugar diet. CWO expression is directly activated by Mondo-Mlx, and it counteracts Myc through repression of its gene expression and through binding to overlapping genomic regions. CWO mouse ortholog BHLHE41 has a conserved role in repressing ribosome biogenesis genes in primary hepatocytes. Collectively, our data uncover a cross-talk between conserved gene regulatory circuits balancing the activities of anabolic pathways to maintain homeostasis during sugar feeding.

INTRODUCTION

Changes in nutrient intake are reflected to organismal metabolism, in part through transcriptional control by nutrient-responsive transcription factors (TFs). High-sugar feeding activates so-called intracellular sugar sensing, mediated by the conserved basic-helix-loop-helix (bHLH) TF Mondo (paralogs ChREBP and MondoA in mammals), heterodimerized with Mlx.[1] Mondo-Mlx controls metabolic pathways, including the activation of genes involved in glycolysis, pentose phosphate pathway, and *de novo* lipogenesis, which collectively promote the conversion of sugars into triacylglycerols.[2] Impaired activation of Mondo/ChREBP-Mlx leads to lethality on high-sugar diet in *Drosophila* and mouse.[3,4]

In addition to nutrient-mediated control of lipid metabolism, protein biosynthesis is tightly regulated by nutrient status, for example through transcriptional control of ribosome biogenesis. A key regulator of ribosome biogenesis is the bHLH TF heterodimer of Myc and Max, which control their target genes through binding to E-box motifs.[5–7] Myc and Max are closely related to Mondo/ChREBP and Mlx, collectively referred to as the "extended Myc network."[8,9] In *Drosophila*, Myc acts downstream of the amino acid-sensing protein kinase mTORC1, activating genes involved in ribosome biogenesis and consequently promoting tissue growth.[5,10] mTORC1 inhibition by amino acid deprivation leads to downregulation of Myc expression, thus repressing ribosome biogenesis gene expression.[5,11]

Despite the parallel roles as drivers of distinct nutrient-responsive metabolic processes, Mondo-Mlx and Myc-Max are functionally interconnected. Myc cooperates with both ChREBP and MondoA by jointly promoting the expression of a subset of target genes.[12,13] In mouse liver, ChREBP cooperates with Myc to promote the expression of ribosomal protein genes.[13] Myc is also known to antagonize the function of MondoA, for example by downregulating the expression of the MondoA target gene *Txnip* in triple-negative breast cancer.[12] In *Drosophila*, *mondo* and *myc* mutants display a synthetic lethal phenotype, implying a joint function.[14] Despite the evidence of functional interplay between Mondo/ChREBP and Myc, it remains to be determined how Mondo and Myc regulate each other's function in a changing nutrient landscape.

Circadian changes in animal physiology are controlled by the core circadian clock, a conserved gene regulatory network, which includes an E-box binding heterodimer of the bHLH TFs Clock and Cycle.[15] Circadian gene expression is modulated by nutrition, and there is tight interplay between the circadian clock

and nutrient sensing.[16] For example, the expression of Cabut/Krüppel-like factor 10 is activated by Mondo/ChREBP-Mlx, and it modulates metabolic gene expression output of the circadian clock.[17,18] Clockwork orange (CWO) is a transcriptional repressor that regulates the core circadian clock by binding to common E-box motifs with Clock and Cycle, thus counteracting their function.[19–22] CWO has two mammalian orthologs, BHLHE40/DEC1 and BHLHE41/DEC2, and they both display repressive roles in the circadian clock,[23,24] similar to that of CWO in *Drosophila*. Moreover, BHLHE40/DEC1 is a direct target of ChREBP in mammalian cells, with a proposed role as a negative regulator of lipogenesis.[25] The metabolic functions of CWO and its contribution to global gene regulation in response to dietary sugar remain to be established.

Here, we identify a regulatory circuit that functionally couples Mondo-Mlx-mediated intracellular sugar sensing and Myc-dependent control of ribosome biogenesis. Following temporal clustering of sugar-responsive gene expression output, we identify a transient sugar-induced repression of genes involved in ribosome biogenesis. Computational prediction of candidate TFs and subsequent experimental analyses uncovered the Mondo-Mlx target TF CWO as a mediator of this repressive response. CWO negatively regulates *myc* gene expression as well as counteracts Myc function through binding of overlapping genomic E-box motifs. Loss of CWO impaired survival on a high-sugar diet along with depletion of uridine diphosphate N-acetylglucosamine (UDP-GlcNAc), a metabolite consumed during ribosome biogenesis. Mammalian orthologs of CWO and BHLHE40 and -41 were identified as direct targets of ChREBP in mouse liver. BHLHE41, but not BHLHE40, negatively regulates ribosome biogenesis gene expression in mouse primary hepatocytes. In conclusion, our data identify a conserved mechanism for cross-talk between major regulators of nutrient-responsive gene expression in multicellular animals.

RESULTS

Temporally and functionally distinct transcriptional outputs to high-sugar feeding

Feeding on a high-sugar diet (HSD) triggers a global transcriptional response in *Drosophila* larvae, which reprograms the metabolic homeostasis of the animals.[2,26] We hypothesized that biologically different transcriptional programs follow distinct activation/attenuation kinetics. Hence, we utilized timed sugar feeding along with unsupervised clustering to identify biological functions for sugar-responsive genes in *Drosophila*.

Larvae of the w^{1118} genotype were reared on a low-sugar diet (LSD; 10% yeast) for 24 h and subsequently transferred to an LSD (10% yeast) for 8 h and an HSD (10% yeast + 20% sucrose) for 4, 8, and 16 h, respectively. Subsequently, RNA sequencing (RNA-seq) was performed, and differentially expressed genes were identified (Figure 1A). Genome wide, 3,085 genes were differentially expressed between animals exposed to an LSD and an HSD, respectively (adjusted p value [adj.p.value] < 0.05; log2 fold change > 0.5 or < −0.5; Table S1). Unsupervised clustering of the genes based on their transcript levels after 4, 8, and 16 h of HSD exposure allowed us to divide the genes into 14 clusters, 7 of which showed general up- ("UP1–7") and downregulation ("DN1–7") after sugar feeding, respectively (Figures 1B and S1). The gene activation patterns included a sustained sugar-induced expression (UP3), a rapid transient upregulation (UP7), and a late response (UP1). Our previous studies have shown the important role of Mondo-Mlx in sugar-induced gene expression.[2] Interestingly, the Mondo-Mlx-dependent target genes were highly (>40%) represented in the UP3 cluster with a sustained sugar-activation pattern but displayed low representation (<5%) in the clusters with transient (UP7) and late (UP1) sugar responses (Figure S2A). This implies that kinetically distinct gene groups are regulated by different TFs.

Cluster UP3 contained genes involved in glycolysis and pyruvate metabolism (Figure 1C), which is in line with the finding of a high percentage of Mondo-Mlx targets (Figures S2A and S2B). The pentose phosphate pathway was enriched in cluster UP3 (Figures 1C and S2B), earlier found to be targeted by Mondo-Mlx.[2] Clusters independent of Mondo-Mlx included the transiently sugar-activated cluster UP7, containing genes involved in endocytosis and autophagy (Figure S2D), and the late-activated cluster UP1, including genes of the electron transport chain (Figures 1C and S2E). A strong enrichment for processes such as "cellular response to starvation," "positive regulation of multicellular organism growth," and "ribosome biogenesis in eukaryotes" was found in the transiently downregulated clusters DN1 and DN3 (Figures 1C, S2F, and S2G). Cluster DN7, with gradual downregulation of genes upon sugar feeding, included genes involved in fatty acid and amino acid catabolism (Figures 1C and S2H). Taken together, the temporal clustering of sugar-regulated genes revealed biologically distinct gene groups, including both Mondo-Mlx-dependent and -independent gene groups.

CWO controls sugar-induced ribosome biogenesis gene regulation

To identify TFs in sugar-responsive gene regulation, we made use of the DREME algorithm,[27] which we set to search for short TF binding motifs enriched in promoter regions of the genes present in the 14 clusters. A strong enrichment of the "CACGTG" E-box motif was observed exclusively in the transiently downregulated gene clusters DN1 and DN3. Comparison with the experimentally validated TF binding sites[28] using TOMTOM[29] predicted CWO as a possible candidate TF binding to these E-box motifs (Figure 1D). Considering the data linking the mammalian ortholog of CWO to sugar-responsive gene regulation,[25] we wanted to test whether CWO is indeed involved in the regulation of genes in clusters DN1 and DN3. Control and *cwo*-null mutant (cwo^{B9}[20]) larvae were exposed for 8 h to an LSD and an HSD, respectively, and RNA-seq was performed to identify CWO-dependent transcriptional changes. A strikingly high percentage of genes in DN1 and DN3 were found to be repressed by sugar in a CWO-dependent manner (Figures 1E, S2I, and S2J). CWO targets were found in much lower percentages in other downregulated clusters and in sugar-activated clusters (Figure S2K).

cwo is necessary for sugar tolerance and maintenance of UDP-GlcNAc pools

Known regulators of sugar-dependent gene expression include Mondo-Mlx, which directly controls the expression of

CellPress
OPEN ACCESS

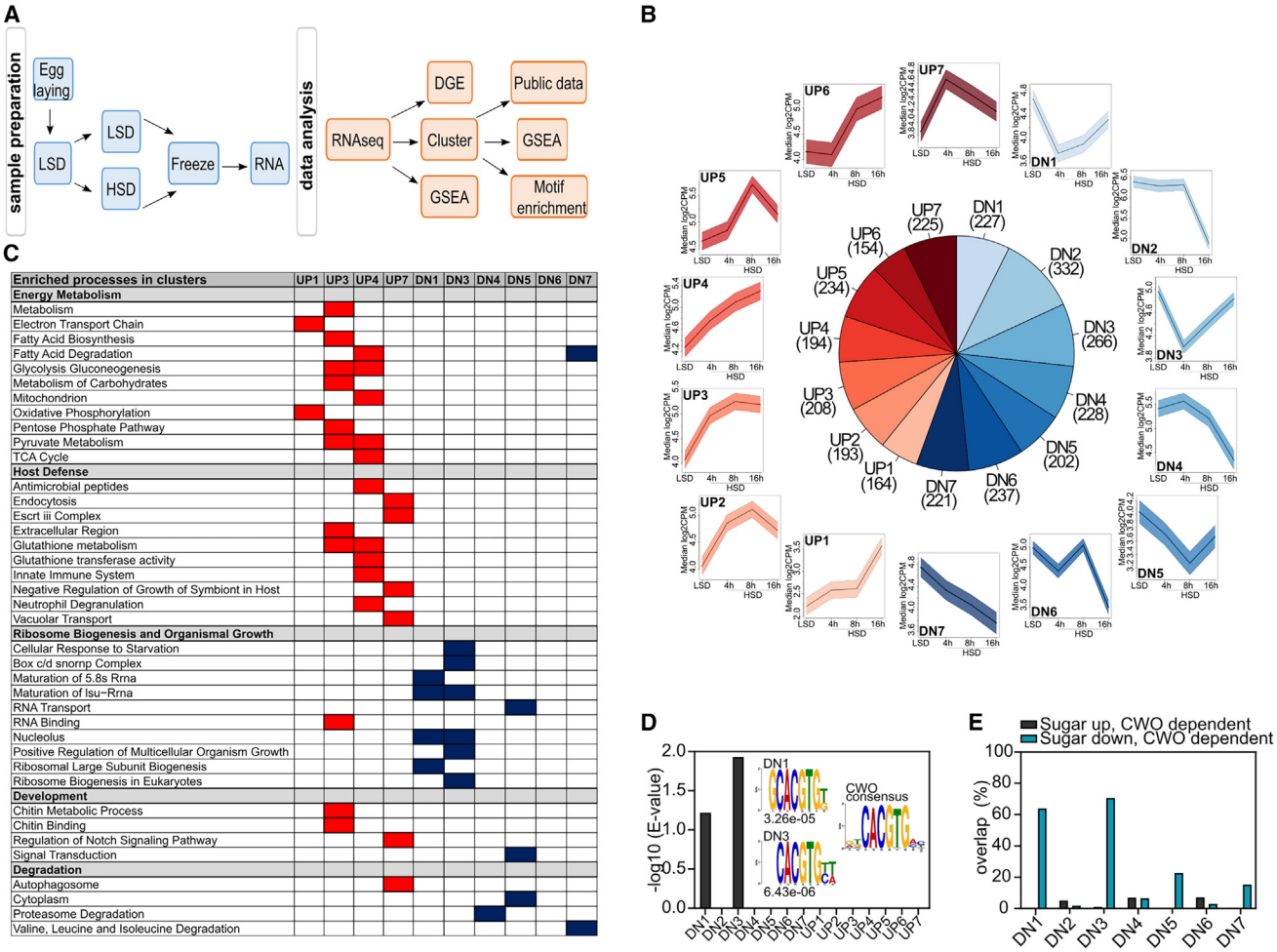

Figure 1. Feeding on high-sugar diet induces temporally distinct gene expression programs

(A) Workflow for the temporal clustering of sugar-responsive gene expression and prediction of TFs involved. Larvae (w^{1118}) were exposed to an LSD and a high-sugar diet (HSD) for 4, 8, and 16 h, respectively (n = 4; 10 larvae/sample; LSD = 10% yeast; HSD = 10% yeast + 15% sucrose), followed by RNA-seq. Differentially regulated genes are listed in Table S1.

(B) Up- and downregulated clusters of HSD-responsive gene expression programs (Fuzzy clustering; adj.p.value < 0.05 in any comparison, LFC<−0.5/LFC>0.5). Genes belonging into each cluster are listed in Table S1. The line depicts the median log2CPM, and the colored line is SEM (standard deviation of mean).

(C) Biological processes enriched in the sugar-regulated gene clusters (gene set enrichment analysis [GSEA]). Red boxes denote pathways that were generally upregulated, and blue boxes downregulated, on an HSD. Genes belonging into each cluster are listed in Table S1.

(D) Enrichment of E-box-like motifs (DREME) in the promoters of genes in clusters DN1 and DN3 as putative binding sites of CWO (TOMTOM). Significant CWO motifs are plotted with the lowest E.value across all clusters.

(E) Enrichment of DN1 and DN3 among genes downregulated by sugar in a CWO-dependent manner. RNA-seq of larvae of the control (ctrl; w^{1118}) and cwo^{B9} genotypes exposed for 8 h to an LSD or an HSD, respectively (n = 4; 10 larvae/sample; LSD = 10% yeast; HSD = 10% yeast + 15% sucrose). RNA-seq identified *cwo*-dependent and sugar-regulated genes (adj.p.value < 0.05). These genes were overlapped with the previously identified 14 clusters revealing a significant overlap with clusters DN1 (64%, adj.p.value = 9.1e−89) and DN3 (71%, adj.p.value = 1.2e−128).

other sugar-responsive TFs, such as Sugarbabe, Cabut, and Grain.[2,3,17,30] We therefore wanted to test whether *cwo* is also a downstream target of Mondo-Mlx or a parallel regulator of sugar-responsive gene expression. The mRNA expression of *cwo* was found to be elevated upon sugar feeding, and this increase was blunted in Mlx-deficient larvae (Figure 2A). Moreover, chromatin immunoprecipitation (ChIP)-qPCR experiments in *Drosophila* S2 cells provided evidence for direct, glucose-stimulated binding of Mlx to the *cwo* promoter (Figure 2B).[17] Furthermore, a putative carbohydrate response element (ChoRE) was identified 1,368 bp upstream of the transcription start site of *cwo* (Figure S3A). Kinetic analysis of *cwo* expression revealed that the sugar-induced expression was elevated at 4 and 8 h time points but attenuated at the 16 h time point (Figure 2C). This might be due to negative autoregulation, supported by the finding that *cwo* mRNA expression was strongly upregulated in the cwo^{B9} mutant, which encodes a severely truncated version of the CWO protein (Figure S3B). Indeed, reanalysis of

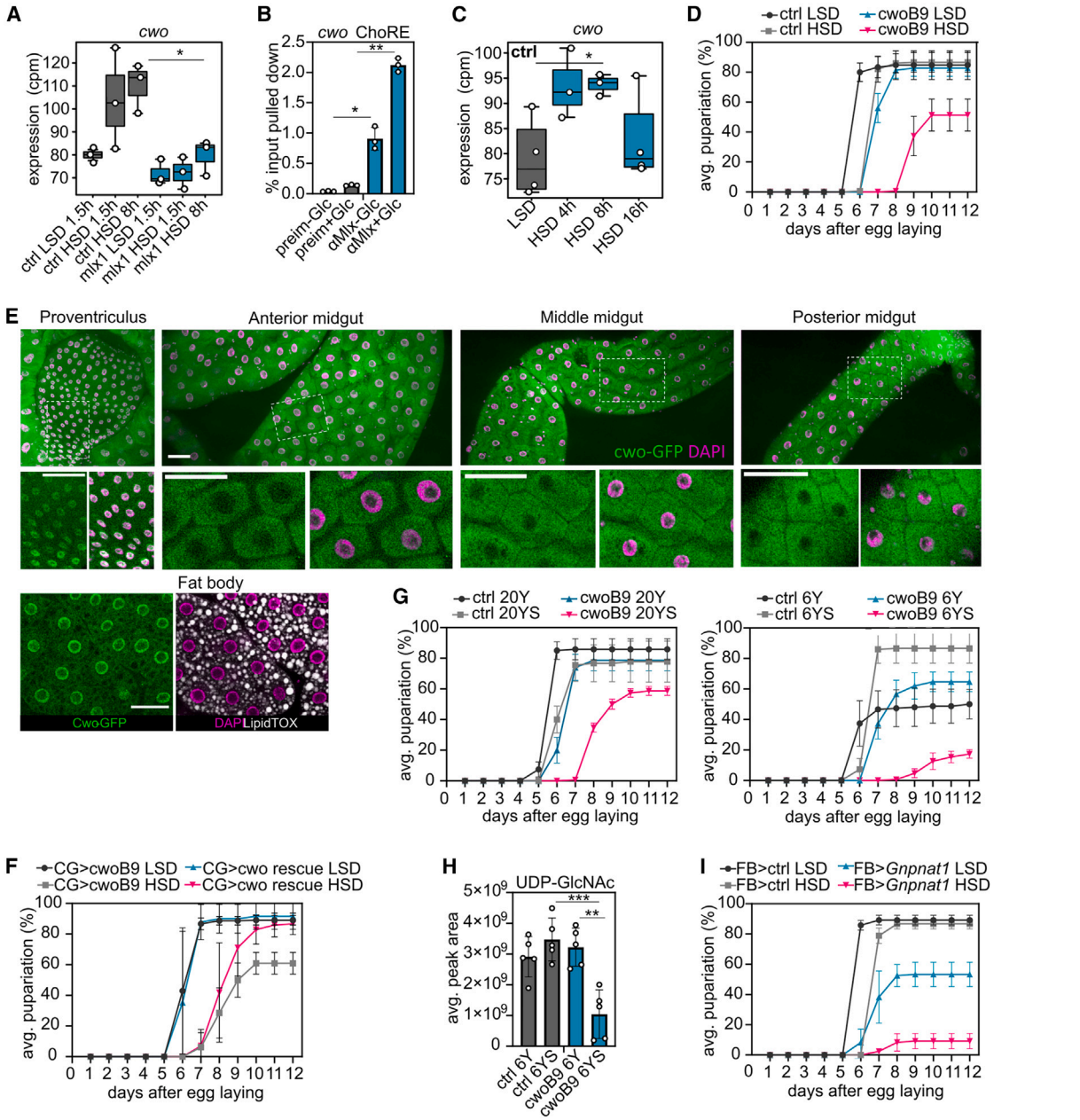

Figure 2. CWO is necessary for sugar tolerance and maintenance of UDP-GlcNAc pools on HSD

(A) *cwo* expression is upregulated upon sugar feeding in an Mlx-dependent manner. RNA-seq of ctrl (w^{1118}) and mlx^1 mutant larvae exposed to an LSD or an HSD for 1.5 or 8 h, respectively (n = 3–4, 10 larvae/sample).

(B) Glucose-inducible binding of Mlx to the *cwo* promoter. Chromatin immunoprecipitation-qPCR in *Drosophila* S2 cells using anti-Mlx antibodies (αMlx) or preimmune serum (preim) in the presence (+Glc) or absence (−Glc) of 50 mM glucose for 6 h (n = 3). Student's t test was used for statistics.

(C) Temporal pattern of *cwo* expression in response to HSD feeding (RNA-seq). Larvae (w^{1118}) were exposed to an LSD and an HSD for 4, 8, and 16 h, respectively.

(D) Delayed pupariation and impaired survival of *cwo* mutant larvae on HSD. Pupariation kinetics of ctrl (w^{1118}) and *cwo*-null mutant (cwo^{B9}) larvae reared on an LSD and an HSD, respectively (n = 5, 30 larvae/sample).

(E) CWO-GFP nuclear localization was observed in the proventriculus and fat body but not in the midgut. CWO-GFP (green), DAPI (magenta), and LipidTOX (lipid droplets, gray) are displayed. Scale bars: 50 μm.

(F) Transgenic CWO in the fat body partially rescues the survival of *cwo* mutant larvae on HSD. Pupariation of *cwo*-deficient ctrl larvae (CG>, cwo^{B9}) and larvae expressing the *cwo* transgenes in the fat body (CG>*cwo* rescue, CG-Gal4>UAS-*cwo*, cwo^{B9}), reared on an LSD and an HSD, respectively (two independent experiments combined; n = 7–10, 30 larvae/sample; CG, CG-Gal4).

(legend continued on next page)

ModENCODE ChIP-seq data on *Drosophila* embryos uncovered strong binding of CWO to its own gene region (Figure S3C). Two perfect E-boxes were found upstream of the *cwo* transcriptional start site (−1,426 and −929 bp) and six in the first intron (+2,194 to +6,142 bp), consistent with the CWO ChIP-seq data.

The cwo^{B9}-null mutants are viable with no known larval phenotypes.[20] As Mondo-Mlx and its targets are necessary for growth and survival on an HSD, we analyzed pupariation of cwo^{B9} mutant larvae on an HSD vs. an LSD. On an LSD, they survived to a similar degree as control larvae, only showing a minor developmental delay (Figure 2D; Table S3). On an HSD, however, the cwo^{B9} mutants displayed a significant developmental delay and only 50% survival to pupal stage (Figures 2D and S3D; Table S3). Additionally, the pupal volume of cwo^{B9} animals on an HSD, but not on an LSD, was reduced (Figure S3E). Adult emergence was moderately compromised on an LSD and severely on an HSD (Figure S3F). An independent loss-of-function strategy, i.e., RNAi-mediated ubiquitous knockdown of *cwo*, replicated the sugar-intolerance phenotype. *cwo* knockdown on an LSD did not affect larval survival, while a strong developmental delay and impaired survival was observed when the animals were exposed to an HSD (Figures S3G and S3H; Table S3).

To characterize the function of CWO further, we utilized the CWO-GFP under the endogenous promoter, allowing detection of tissue-specific expression and localization of CWO by fluorescence microscopy. To avoid autofluorescence caused by yeast-based diets, we exposed third instar CWO-GFP/+ larvae for 6 h to a holidic diet, followed by dissection and imaging of the larval tissues. CWO-GFP signals were found in the midgut and the fat body, important tissues for maintaining sugar tolerance. Interestingly, however, CWO displayed nuclear localization in the fat body but not in enterocytes (Figure 2E), consistent with transcriptional activity in the fat body but not in enterocytes. Indeed, a genetic rescue experiment revealed that its function in the enterocytes was not sufficient to rescue sugar intolerance of *cwo* mutants (Figure S3I). In contrast, transgenic *cwo* expression in the fat body led to a partial rescue: while only 60% of cwo^{B9} mutant animals pupariated on an HSD, a statistically significant increase of pupariation rate was observed (Figures 2F and S3J; Table S3). However, the developmental delay was not rescued by fat body-specific CWO expression, indicating that a yet unidentified additional organ might contribute to CWO-dependent sugar tolerance.

As the genes enriched in clusters DN1 and DN3 are involved in promoting growth and are downregulated by nutrient starvation, we tested whether the sugar-intolerance phenotype of *cwo* mutants was affected by changes in the availability of dietary yeast, containing nutrients essential for growth. Indeed, the sugar-intolerance phenotype caused by 15% dietary sucrose was strongly exacerbated on a diet with low (6%) yeast compared with a high-yeast (20%) diet (Figure 2G; Table S3). In contrast, survival of control animals on a low-yeast diet was improved by the addition of sucrose (Figures 2G, S3K, and S3L; Table S3) due to reasons that remain to be elucidated. To further characterize the role of CWO in physiological adaptation to an HSD, we analyzed metabolic phenotypes and feeding behavior. Loss of CWO did not cause significant changes in total triacylglycerol levels (Figure S3M) or food intake (Figure S3N). Global metabolomics analysis of polar metabolites was conducted on conditions of low (6%) yeast supplemented, or not, with 15% sucrose (Figures S3O and S3P). Prominent accumulation of urate, a breakdown product of purine nucleotides, was observed (Figure S3Q). Moreover, levels of UDP-GlcNAc were strongly reduced in *cwo* mutants, specifically on an HSD (Figure 2H), implying that CWO is necessary to maintain sufficient UDP-GlcNAc pools on an HSD. Does maintenance of UDP-GlcNAc pools contribute to sugar tolerance? To test this, we inhibited the hexosamine biosynthesis pathway by fat body-specific (FB-GAL4>) knockdown of glucosamine-phosphate N-acetyltransferase (*Gnpnat*). Indeed, *Gnpnat* knockdown strongly impaired the survival of larvae on an HSD (Figure 2I; Table S3).

CWO and its mouse orthologs regulate the expression of ribosome biogenesis genes

Our larval RNA-seq analysis demonstrated a role for CWO in the sugar-responsive repression of growth-promoting genes, many of which are involved in ribosome biogenesis. Interestingly, ribosome biogenesis is known to be dependent on cellular UDP-GlcNAc pools, and the enzymes that conjugate and deconjugate O-GlcNAc are associated with the ribosomes, and several ribosomal proteins are modified by O-GlcNAcylation.[31] Thus, it is possible that CWO maintains UDP-GlcNAc pools by controlling the activity of ribosome biogenesis. Consistent with the clustering data, gene set enrichment analysis of the cwo^{B9} RNA-seq data revealed significant enrichment of "ribosome biogenesis in eukaryotes." The genes involved in ribosome biogenesis displayed a strong downregulation upon sugar feeding, which was significantly compromised, albeit not completely prevented, in *cwo* mutants (Figure 3A). Expression of several ribosome biogenesis genes is inhibited upon nutrient starvation or rapamycin treatment, including *Nop60B*, *Mat89Ba*, and *ppan*.[5,11] *Nop60B*, *Mat89Ba*, and *ppan* were studied further,

(G) Sugar intolerance of *cwo* mutants is aggravated by reduction of dietary yeast. Pupariation of ctrl (w^{1118}) and *cwo*-null mutant (cwo^{B9}) larvae reared on a 20% yeast (left panel) and 6% yeast (right panel) diet in the presence or absence of 15% sucrose, respectively (n = 3–5; 30 larvae/sample). 20Y, 20% yeast; 20YS, 20% yeast + 15% sucrose; 6Y, 6% yeast; 6YS, 6% yeast + 15% sucrose.

(H) UDP-GlcNAc levels are downregulated in *cwo* mutants on diet with low yeast (6%) and high sucrose (15%). Ctrl (w^{1118}) and cwo^{B9} larvae were exposed to a low-yeast diet in the presence or absence of 15% sucrose for 24 h (n = 5; 20 larvae/sample; 6Y, 6% yeast; 6YS, 6% yeast + 15% sucrose). Two-way ANOVA was used for statistics.

(I) Inhibition of the hexosamine pathway in the larval fat body (FB>*gnpnat1* RNAi) leads to impaired pupariation on HSD. Pupariation of ctrl larvae (FB>ctrl; ctrl, Trip Val20 ctrl, Bl.#36303) and larvae expressing a *Gnpnat1* RNAi in the FB (FB>*Gnpnat1* RNAi, Bl.#50616) on an LSD and an HSD, respectively (n = 3–4; 30 larvae/sample; FB, FB-Gal4).

CPM, counts per million; LSD, 10% yeast; HSD, 10% yeast + 15% sucrose. Data are shown as individual data points and mean ± standard deviations; selected comparisons are displayed as *p < 0.05, **p < 0.01, and ***p < 0.001; all p values for comparisons displayed can be found in Table S2. Statistics for pupariation index data can be found in Table S3.

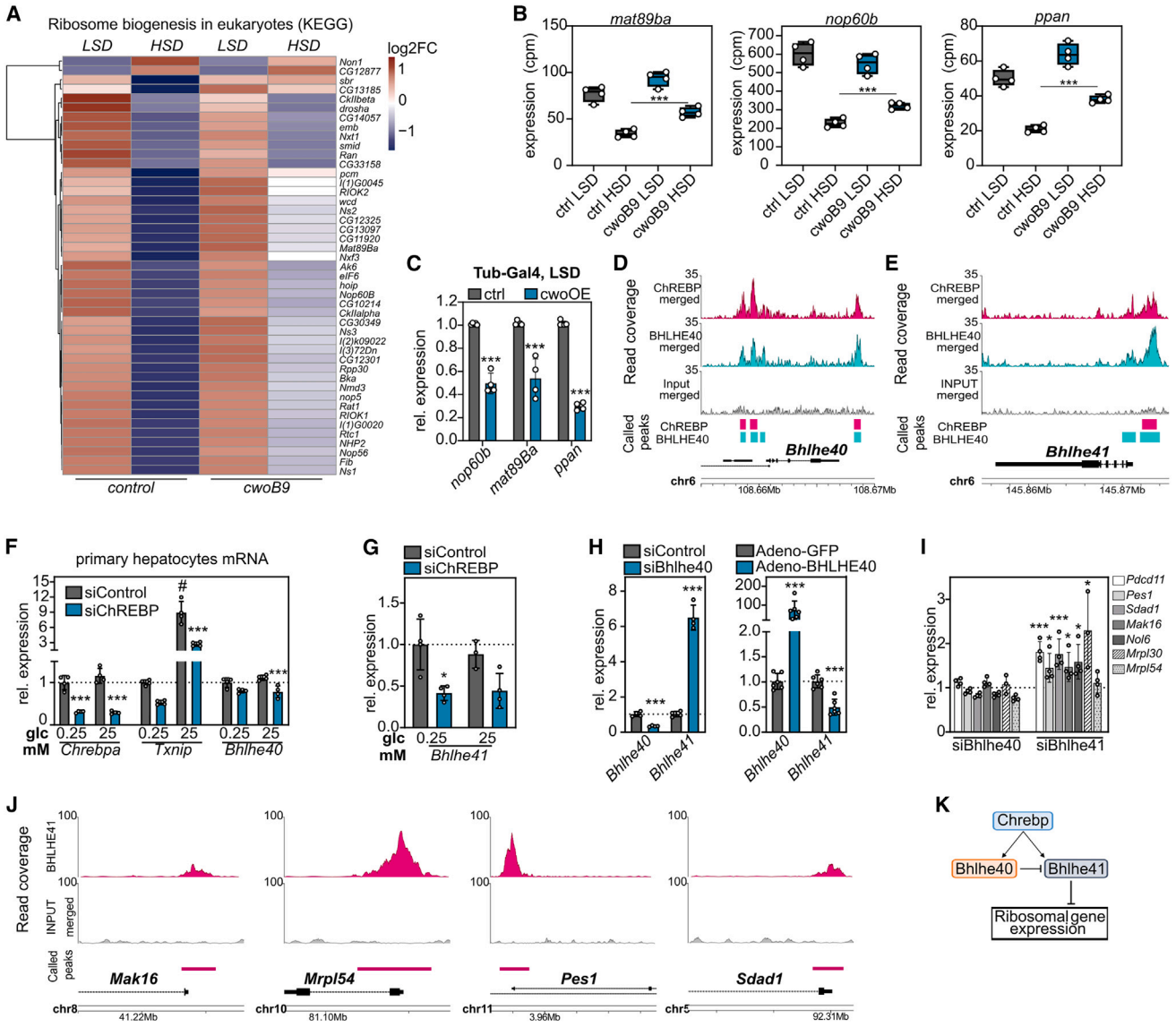

Figure 3. CWO and its mouse ortholog BHLHE41 repress ribosome biogenesis genes

(A) Sugar-induced downregulation of "ribosome biogenesis in eukaryotes" (KEGG) is partially blunted in *cwo* mutant larvae (GSEA). The row-wise clustering was performed using correlation distance. Color key displays scaled log2 gene expression.

(B) *cwo* loss of function suppressed the sugar-induced downregulation of ribosome biogenesis genes *Nop60B*, *Mat89Ba*, and *ppan.* RNA-seq of ctrl (w^{1118}) and cwo^{B9} larvae (n = 4; 10 larvae/sample).

(C) Ubiquitous overexpression of *cwo* (Tub>*cwo*OE [overexpression]) on LSD leads to reduced expression of *Nop60B*, *Mat89Ba*, and *ppan* (n = 4–5, 10 larvae/sample). Student's t test was used for statistics.

(D) ChREBP and BHLHE40 binding near the *Bhlhe40* gene locus in liver via ChIP-seq of C57Bl/6 male mice (n = 2 for ChREBP, BHLHE40, and input ctrl, respectively). Merged ChIP-seq binding profiles and called peak locations (q value < 0.05) are displayed. Pink: ChREBP, turquoise: BHLHE40.

(E) ChREBP and BHLHE40 binding near the *Bhlhe41* gene in mouse liver. Merged ChIP-seq binding profiles and called peak locations (q value < 0.05) are displayed. Pink: ChREBP, turquoise: BHLHE40.

(F) Knockdown of ChREBP in primary mouse hepatocytes reduced the expression (qPCR) of known ChREBP target genes *Txnip* and *Bhlhe40.* Primary mouse hepatocytes with siControl or siChREBP were exposed to 0.25 or 25 mM glucose (glc) for 8 h (n = 4). mRNA expression displayed as relative expression to siControl 0.25 mM glc. One-way ANOVA + Tukey post hoc test was used for statistics.

(G) Knockdown of ChREBP in primary mouse hepatocytes reduced the expression (qPCR) of *Bhlhe41.* Primary mouse hepatocytes with siControl or siChREBP were exposed to 0.25 or 25 mM glc for 8 h (n = 3–4). mRNA expression was displayed as relative expression to siControl 0.25 mM glc. One-way ANOVA + Tukey post hoc test was used for statistics.

(H) Knockdown and overexpression of BHLHE40 in primary mouse hepatocytes resulted in a transcriptional (qPCR) up- and downregulation, respectively, of *Bhlhe41*. Primary mouse hepatocytes with siControl and siBhlhe40 or infected with adenoviruses expressing GFP or BHLHE40 were exposed to 25 mM glc for 72 h (n = 4). Student's t test (two-tailed) was used for statistics.

(legend continued on next page)

serving as examples for the behavior of this class of genes. They were found to be downregulated on an HSD in control animals, but the downregulation was partially blunted in *cwo* mutants (Figure 3B), while overexpression of CWO on an LSD led to significant downregulation (Figure 3C), implicating CWO as a transcriptional regulator of *Nop60B*, *Mat89Ba*, and *ppan*. Although the expression of ribosome biogenesis genes was also inhibited upon full starvation[32] (Figures S4A and S4B), this occurred independently of *cwo* upregulation (Figure S4C). Thus, CWO-mediated inhibition of ribosome biogenesis genes is specific to an HSD and is not likely to reflect reduced intake of amino acids.

In order to address the possible conservation of CWO's regulation and function, we analyzed mouse liver and primary murine hepatocytes. *Drosophila* CWO has two mammalian orthologs, BHLHE40 and BHLHE41. ChIP-seq on mouse liver revealed genomic-binding sites of ChREBP, the ortholog of *Drosophila* Mondo, and also of BHLHE40 up- and downstream of the *Bhlhe40* locus (Figure 3D). Moreover, both ChREBP and BHLHE40 bind regions upstream of the *Bhlhe41* gene (Figure 3E). To investigate the hierarchical relationship between these factors in more detail, small interfering RNA (siRNA)-mediated knockdown was performed in mouse primary hepatocytes. Figure 3F shows the expected ChREBP-dependent induction of *Txnip* expression by high-glucose concentrations.[33] Consistent with earlier findings,[25] expression of *Bhlhe40* was inhibited by knockdown of ChREBP. Moreover, knockdown of ChREBP led to downregulation of *Bhlhe41*, in line with our ChIP-seq data on mouse livers (Figure 3G). As *Bhlhe41* was identified as a direct target of BHLHE40, we wanted to functionally test the role of BHLHE40 in the regulation of *Bhlhe41* expression. Consistent with a repressive role of BHLHE40 on *Bhlhe41*, as shown earlier by BHLHE40 overexpression in the 293T cell line,[34] knockdown of *Bhlhe40* increased and overexpression decreased expression of *Bhlhe41,* respectively (Figure 3H). Despite the observed repressive function of BHLHE40 on *Bhlhe41*, the downregulation of *Bhlhe40* was not sufficient to prevent the downregulation of *Bhlhe41* upon ChREBP knockdown (Figure 3G). Since BHLH40 and BHLHE41 have been reported to have partially overlapping functions in immune cells, like activated macrophages[35,36] and T cells,[37–39] we tested whether either factor controls ribosomal gene expression. We found that knockdown of *Bhlhe41*, but not of *Bhlhe40*, caused an upregulation of ribosomal gene expression (Figure 3I), many of which were found to be direct targets of BHLHE41 (Figure 3J). Taking into account the upregulation of *Bhlhe41* upon BHLHE40 knockdown, we conclude that BHLHE41 is necessary, but not sufficient, to repress ribosomal gene expression.

Taken together, our results suggest that both *Bhlhe40* and *Bhlhe41* are downstream targets of ChREBP and that BHLHE40 has a repressive effect on *Bhlhe41*. BHLHE41, but not BHLHE40, negatively regulates ribosomal gene expression in murine hepatocytes (Figure 3K), similar to the function of CWO in *Drosophila*.

CWO functionally antagonizes MYC

To further address the mechanism of CWO-mediated repression of ribosome biogenesis genes, we turned our attention to Myc, a known positive regulator of ribosome biogenesis.[5] Interestingly, our reanalysis of ModENCODE ChIP-seq data showed prominent binding of CWO in the first intron of the *myc* gene, suggesting that *myc* is a direct target of CWO (Figure 4A). Moreover, overexpression of *cwo* in the LSD condition led to a significant decrease of *myc* transcript levels compared with the control (Figure 4B). Consistently, *myc* expression was upregulated in *cwo* mutants on both dietary conditions (Figure 4C) while being modestly downregulated in a sugar-dependent manner in controls but not *cwo* mutant flies (Figure 4C). In contrast to *Drosophila* Myc, the expression of mouse Myc was unchanged upon knockdown of BHLHE41, and we found no evidence for mouse BHLHE41 binding near the *myc* gene (Figures S4D and S4E; Table S3). To test the role of Myc expression on larval sugar tolerance, we exposed larvae overexpressing *myc* in the FB to an LSD and an HSD, respectively (Figure 4D; Table S3). The *myc*-overexpressing animals displayed a delayed development on the HSD, reduced pupariation, and adult emergence (Figures S4F and S4G), demonstrating that high Myc expression in the FB is sufficient to sensitize larvae to an HSD (Figure 2D). Given the modest transcriptional downregulation of the *myc* gene upon sugar feeding, we wanted to test whether transcriptional regulation of *myc* is sufficient to explain all of the observed inhibition of ribosome biogenesis genes. We utilized a genetic setup with the endogenous *myc* gene replaced by a transgenic version and observed that ribosome biogenesis genes displayed downregulation on the HSD even in the transgenic rescue lines (Figure S4H).

As transcriptional regulation of endogenous *myc* gene was not sufficient to fully explain the observed sugar-responsive repression, we further analyzed the interplay between CWO and Myc at the promoters of ribosome biogenesis genes. Consistent with the fact that both Myc and CWO bind to E-box motifs, we found a strong enrichment of predicted Myc binding sites in CWO target clusters, DN1 and DN3 (E value [E.val] < 0.01). Myc is known to directly regulate *Nop60B*, *Mat89Ba*, and *ppan*,[5] which we found to be regulated by CWO (Figures 3B and 3C). Therefore, we systematically compared genomic-binding sites of CWO with MYC in the available ChIP-seq data on *Drosophila* embryos. This analysis revealed a striking overlap of CWO and Myc genomic-binding sites, even with a highly stringent

(I) Knockdown of BHLHE41, but not BHLHE40, led to an induction of ribosomal gene expression (qPCR) in primary mouse hepatocytes. Primary mouse hepatocytes transfected with siBhlhe40 or siBhlhe41 were exposed to 25 mM glc for 72 h (n = 3–4). mRNA expression was displayed as relative expression to siControl = 1. One-way ANOVA + Tukey post hoc test was used for statistics.

(J) BHLHE41 binding near selected ribosome biogenesis genes in mouse B-1a cells (GEO: GSE93764). Merged ChIP-seq binding profiles and called peak locations (q value < 0.05) are displayed.

(K) A model for ChREBP-BHLHE40-BHLHE41 interactions and the regulation of ribosomal gene expression.

CPM, counts per million; LSD, 10% yeast; HSD, 10% yeast + 15% sucrose. Data are shown as individual data points and mean ± standard deviations; selected comparisons are displayed as *p < 0.05, **p < 0.01, and ***p < 0.001; all p values for comparisons can be found in Table S2.

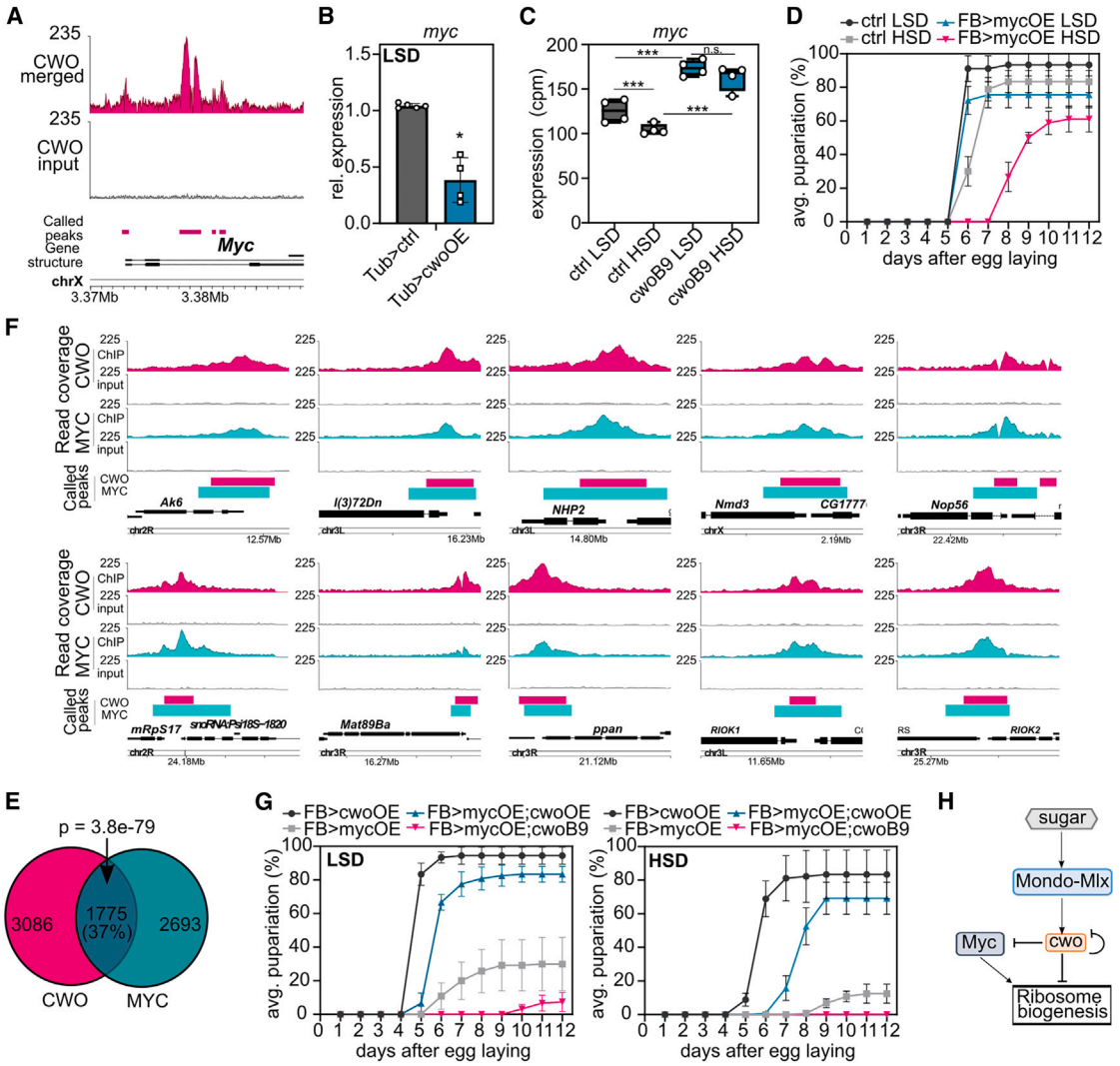

Figure 4. CWO functionally antagonizes Myc

(A) CWO binding to *myc* gene locus. Reanalysis of *Drosophila* embryo ChIP-seq data (ENCODE: ENCSR900TNL). Data are displayed as average signal intensity, MACS2-called peaks marked as pink bars (n = 3). Merged ChIP-seq binding profiles and called peak locations (q value < 0.05) are displayed.

(B) Ubiquitous *cwo* OE downregulates *myc* expression in larvae on LSD. Ctrl larvae (Tub>ctrl; ctrl, FlyORF ctrl) and *cwo* overexpressing larvae (Tub>cwoOE; cwoOE, FlyORF F000668) on an LSD (qPCR; n = 4–5, 10 larvae/sample). Student's t test was used for statistics (Tub, tubulin-Gal4).

(C) Upregulation of *myc* expression in *cwo* mutant larvae. RNA-seq of ctrl (w^{1118}) and cwo^{B9} larvae (n = 4; 10 larvae/sample).

(D) *myc* OE in the larval FB (FB>*myc*OE) delayed pupariation and reduced survival on HSD. Representative pupariation kinetics of ctrl larvae (FB>ctrl; ctrl, FlyORF ctrl) and larvae overexpressing *myc* in the FB (FB>*myc*OE) were reared on an LSD and an HSD, respectively (n = 3; 30 larvae/sample; FB, FB-Gal4).

(E) CWO and MYC share 1,775 highly overlapping (>50%) genomic-binding sites. Raw data derived from ENCODE (CWO dataset: ENCSR900TNL, MYC dataset: ENCSR999ZCR, n = 3).

(F) Examples of overlapping CWO and MYC binding motifs in the enriched pathway "ribosome biogenesis in eukaryotes" (KEGG). Reanalysis of publicly available ChIP-seq data (CWO: ENCSR900TNL; MYC: ENCSR999ZCR). Merged ChIP-seq binding profiles and called peak (q value < 0.05) locations are displayed. Pink: ChREBP, turquoise: BHLHE40.

(G) Pupariation of animals overexpressing *myc* in the FB (FB>*myc*OE), displaying either an increase of (FB>*myc*OE; *cwo*OE) or being deficient (FB>*myc*OE;cwo^{B9}) in *cwo* expression. Larvae were reared on an LSD (left) and an HSD (right), respectively (n = 3–5, 30 larvae/sample; FB, FB-Gal4).

(H) A model of CWO-Myc interplay in controlling the transcription of ribosome biogenesis genes.

CPM, counts per million; LSD, 10% yeast; HSD, 10% yeast + 15% sucrose. Data are shown as individual data points and mean ± standard deviations; selected comparisons are displayed as *p < 0.05, **p < 0.01, and ***p < 0.001; all p values for comparisons displayed in this figure and Figures S3 and S4 are shown in Table S2. Statistics for pupariation indexes are displayed in Table S3.

requirement of 50% overlap between the peaks (Figure 4E). The analysis of a number of individual binding sites of CWO and MYC at the promoters of ribosome biogenesis genes revealed almost completely overlapping peaks (Figure 4F), consistent with overlapping binding sites. To functionally test whether CWO can modify the phenotype of Myc, independently of its endogenous expression, we overexpressed transgenic Myc in the FB in the *cwo* mutant as well as upon CWO overexpression. Loss of CWO led to striking enhancement of the Myc gain-of-function phenotype on both the HSD and the LSD (Figure 4G; Table S3), while overexpression of CWO prominently suppressed the Myc phenotype. These data are consistent with the model that CWO functionally antagonizes Myc function in addition to the negative regulation of endogenous *myc* gene expression in *Drosophila* (Figure 4H).

DISCUSSION

This study uncovers CWO, a bHLH TF, as a sugar-induced repressor of ribosome biogenesis genes. CWO serves as a regulatory link between the intracellular sugar sensor Mondo-Mlx and the growth-promoting regulator of ribosome biogenesis Myc. These findings extend the previous literature on the complex cross-talk between Mondo/ChREBP-Mlx and Myc as well as the previous findings of Myc as a regulator of carbohydrate metabolism.[40] In light of the findings reported by Parisi and coworkers, showing Myc-dependent control of carbohydrate and lipid metabolism, it will be interesting to expand the analysis of Mondo-Mlx and Myc cross-talk to explore the contribution of Myc in sugar-responsive control of energy metabolism.

Our findings also strengthen the previously identified connection between intracellular sugar sensing and the circadian clock.[17] Myc expression is regulated in a circadian manner,[41] and high Myc expression disrupts the circadian clock in tumor cells[42] as well as in *Drosophila*, where Myc expression can upregulate the expression of CWO.[43] Together with our data, these findings suggest a two-way interplay between Myc and CWO and indicate that the nutrient-induced control of the CWO-Myc axis might contribute to the adjustment of the circadian clock. Our findings on CWO's ability to counteract Myc function, as well as the widespread overlap between genomic-binding sites of CWO and Myc, raise the possibility for the involvement of CWO in other Myc-dependent processes, including clonal cell competition,[44] which remains to be explored. Experiments in mouse hepatocytes revealed both CWO orthologs (BHLHE40 and BHLHE41) as ChREBP (Mondo ortholog) targets. While BHLHE40/DEC1 has been suggested earlier as a negative feedback regulator of ChREBP-mediated lipogenesis,[25] our gene expression data on CWO do not support functional conservation of this role in *Drosophila*. Instead, we observed that BHLHE41/DEC2 serves as a negative regulator of ribosome biogenesis in mouse hepatocytes, consistent with functional conservation between CWO and BHLHE41. Notably, ribosome biogenesis gene expression is controlled by the circadian clock in the mouse liver.[45] It will be interesting to explore whether the role of ChREBP-mediated sugar sensing through the control BHLHE41 is able to modulate circadian control of ribosome biogenesis.

Inhibition of ribosome biogenesis by nutrient deprivation is well established.[5,46] Our findings on the inhibition of ribosome biogenesis upon acute increase of dietary sugar might seem counterintuitive. However, earlier studies have uncovered an unexpected coupling between ribosome biogenesis and lipid homeostasis. Impaired ribosome biogenesis leads to accumulation of lipid droplets in *C. elegans*.[47] In obese mice, nucleomethylin inhibits ribosomal RNA expression in the liver, which is necessary for the biosynthesis and accumulation of hepatic lipids.[48] Considering the acute need to increase lipid biosynthesis during high-sugar feeding, it might be necessary to downregulate other energy-consuming anabolic pathways, such as ribosome biogenesis, to secure the supply of key metabolites. One such metabolite is UDP-GlcNAc, which is heavily conjugated to ribosome subunits and regulators of ribosome biogenesis[31,49–51] and, based on our data, is necessary for maintaining larval survival on an HSD. In conclusion, this study uncovers dynamic genome-wide interplay between conserved bHLH TFs, which contributes to metabolic homeostasis and viability upon changing dietary sugar intake.

Limitations of the study

Although our data show that CWO controls the output of Myc-dependent ribosome biogenesis on an HSD by inhibiting *myc* gene expression as well as directly binding to overlapping genomic sites, the molecular details of their interaction on target promoters remain to be resolved. The current *in vivo* work focuses on *Drosophila* larvae. Whether the Mondo-Mlx-mediated control of CWO and its influence on the output of Myc contributes to the physiology of adult animals is yet unresolved. Loss of CWO activity leads to depletion of UDP-GlcNAc on an HSD. We propose that failure of the inhibition of ribosome biogenesis might contribute to this depletion, but this hypothesis remains to be tested in future studies.

STAR★METHODS

Detailed methods are provided in the online version of this paper and include the following:

- KEY RESOURCES TABLE
- RESOURCE AVAILABILITY
  - Lead contact
  - Materials availability
  - Data and code availability
- EXPERIMENTAL MODEL AND STUDY PARTICIPANT DETAILS
  - *Drosophila* lines and husbandry
  - Mouse hepatocyte culture and treatments
- METHOD DETAILS
  - Analysis of pupariation and growth
  - RNAseq and related data analysis
  - Temporal clustering of gene expression
  - Gene set enrichment
  - Prediction of candidate TF regulators
  - ChIP and related data analysis
  - Metabolomics
  - Triacylglycerol measurements

- Analysis of food consumption
- Quantitative RT-PCR
- Microscopic analysis of tissues
- Data analysis and visualization

- QUANTIFICATION AND STATISTICAL ANALYSIS

SUPPLEMENTAL INFORMATION

Supplemental information can be found online at https://doi.org/10.1016/j.celrep.2023.112739.

ACKNOWLEDGMENTS

We thank François Rouyer, the Bloomington *Drosophila* Stock Center, the Vienna *Drosophila* Resource Center, and the Zurich ORFeome Project for fly stocks. We thank Heini Lassila, Juhana Juutila, Jack Morikka, Corinna Biermeier, and Annele Holla for technical assistance. Funding was provided by the Academy of Finland through MetaStem Center of Excellence funding to V.H. (312439), the Sigrid Jusélius Foundation (V.H.), the Erkko Foundation (V.H.), and the Novo Nordisk Foundation (NNF18OC0034406, NNF19OC0057478, and NNF22OC0078419 to V.H.), as well as by the German Research Foundation (DFG) SCHU-2546/7-1 to M.S. and WO 2624/1-1 to S.J.W. K.M.P. was supported by the Sonnenfeld Foundation, Berlin. This study was facilitated by the University of Helsinki *Drosophila* core facility (Hi-Fly), the DNA sequencing and genomics core facility, and the Light Microscopy Unit, all supported by Biocenter Finland and Helsinki Institute of Life Science.

AUTHOR CONTRIBUTIONS

Conceptualization, L.v.d.B., K.K., M.S., and V.H.; methodology, A.I.N.; formal analysis, L.v.d.B., K.K., V.H., and R.G.M.; investigation, L.v.d.B., S.J.W., K.M.P., O.D., C.A.S., M.R., and M.T.; writing – original draft, L.v.d.B., K.K., M.S., and V.H.; writing – review & editing, L.v.d.B., K.K., S.J.W., O.D., M.S., and V.H.; visualization, L.v.d.B. and K.K.; supervision, M.S. and V.H.; project administration, V.H.; funding acquisition, M.S. and V.H.

DECLARATION OF INTERESTS

The authors declare no competing interests.

INCLUSION AND DIVERSITY

We support inclusive, diverse, and equitable conduct of research.

Received: July 1, 2022
Revised: May 25, 2023
Accepted: June 19, 2023
Published: July 4, 2023

REFERENCES

1. Havula, E., and Hietakangas, V. (2012). Glucose sensing by ChREBP/MondoA-Mlx transcription factors. Semin. Cell Dev. Biol. *23*, 640–647. https://doi.org/10.1016/j.semcdb.2012.02.007.
2. Mattila, J., Havula, E., Suominen, E., Teesalu, M., Surakka, I., Hynynen, R., Kilpinen, H., Väänänen, J., Hovatta, I., Käkelä, R., et al. (2015). Mondo-Mlx mediates organismal sugar sensing through the Gli-similar transcription factor sugarbabe. Cell Rep. *13*, 350–364. https://doi.org/10.1016/j.celrep.2015.08.081.
3. Havula, E., Teesalu, M., Hyötyläinen, T., Seppälä, H., Hasygar, K., Auvinen, P., Orešič, M., Sandmann, T., and Hietakangas, V. (2013). Mondo/ChREBP-Mlx-regulated transcriptional network is essential for dietary sugar tolerance in Drosophila. PLoS Genet. *9*, e1003438. https://doi.org/10.1371/journal.pgen.1003438.
4. Iizuka, K., Bruick, R.K., Liang, G., Horton, J.D., and Uyeda, K. (2004). Deficiency of carbohydrate response element-binding protein (ChREBP) reduces lipogenesis as well as glycolysis. Proc. Natl. Acad. Sci. USA *101*, 7281–7286. https://doi.org/10.1073/pnas.0401516101.
5. Teleman, A.A., Hietakangas, V., Sayadian, A.C., and Cohen, S.M. (2008). Nutritional control of protein biosynthetic capacity by insulin via Myc in Drosophila. Cell Metab. *7*, 21–32. https://doi.org/10.1016/j.cmet.2007.11.010.
6. Hulf, T., Bellosta, P., Furrer, M., Steiger, D., Svensson, D., Barbour, A., and Gallant, P. (2005). Whole-genome analysis reveals a strong positional bias of conserved dMyc-dependent E-boxes. Mol. Cell Biol. *25*, 3401–3410. https://doi.org/10.1128/MCB.25.9.3401-3410.2005.
7. Zielke, N., Vähärautio, A., Liu, J., Kivioja, T., and Taipale, J. (2022). Upregulation of ribosome biogenesis via canonical E-boxes is required for Myc-driven proliferation. Dev. Cell *57*, 1024–1036.e5. https://doi.org/10.1016/j.devcel.2022.03.018.
8. McFerrin, L.G., and Atchley, W.R. (2011). Evolution of the Max and Mlx networks in animals. Genome Biol. Evol. *3*, 915–937. https://doi.org/10.1093/gbe/evr082.
9. Dang, C.V. (2015). Web of the extended Myc network captures metabolism for tumorigenesis. Cancer Cell *27*, 160–162. https://doi.org/10.1016/j.ccell.2015.01.004.
10. Grewal, S.S., Li, L., Orian, A., Eisenman, R.N., and Edgar, B.A. (2005). Myc-dependent regulation of ribosomal RNA synthesis during Drosophila development. Nat. Cell Biol. *7*, 295–302. https://doi.org/10.1038/ncb1223.
11. Guertin, D.A., Guntur, K.V.P., Bell, G.W., Thoreen, C.C., and Sabatini, D.M. (2006). Functional genomics identifies TOR-regulated genes that control growth and division. Curr. Biol. *16*, 958–970. https://doi.org/10.1016/j.cub.2006.03.084.
12. Carroll, P.A., Diolaiti, D., McFerrin, L., Gu, H., Djukovic, D., Du, J., Cheng, P.F., Anderson, S., Ulrich, M., Hurley, J.B., et al. (2015). Deregulated Myc requires MondoA/Mlx for metabolic reprogramming and tumorigenesis. Cancer Cell *27*, 271–285. https://doi.org/10.1016/j.ccell.2014.11.024.
13. Wang, H., Dolezal, J.M., Kulkarni, S., Lu, J., Mandel, J., Jackson, L.E., Alencastro, F., Duncan, A.W., and Prochownik, E.V. (2018). Myc and ChREBP transcription factors cooperatively regulate normal and neoplastic hepatocyte proliferation in mice. J. Biol. Chem. *293*, 14740–14757. https://doi.org/10.1074/jbc.RA118.004099.
14. Billin, A.N., and Ayer, D.E. (2006). The Mlx network: evidence for a parallel Max-like transcriptional network that regulates energy metabolism. Curr. Top. Microbiol. Immunol. *302*, 255–278. https://doi.org/10.1007/3-540-32952-8_10.
15. Allada, R., and Chung, B.Y. (2010). Circadian organization of behavior and physiology in Drosophila. Annu. Rev. Physiol. *72*, 605–624. https://doi.org/10.1146/annurev-physiol-021909-135815.
16. Zheng, X., and Sehgal, A. (2010). AKT and TOR signaling set the pace of the circadian pacemaker. Curr. Biol. *20*, 1203–1208. https://doi.org/10.1016/j.cub.2010.05.027.
17. Bartok, O., Teesalu, M., Ashwall-Fluss, R., Pandey, V., Hanan, M., Rovenko, B.M., Poukkula, M., Havula, E., Moussaieff, A., Vodala, S., et al. (2015). The transcription factor Cabut coordinates energy metabolism and the circadian clock in response to sugar sensing. EMBO J. *34*, 1538–1553. https://doi.org/10.15252/embj.201591385.
18. Iizuka, K., Takeda, J., and Horikawa, Y. (2011). Kruppel-like factor-10 is directly regulated by carbohydrate response element-binding protein in rat primary hepatocytes. Biochem. Biophys. Res. Commun. *412*, 638–643. https://doi.org/10.1016/j.bbrc.2011.08.016.
19. Matsumoto, A., Ukai-Tadenuma, M., Yamada, R.G., Houl, J., Uno, K.D., Kasukawa, T., Dauwalder, B., Itoh, T.Q., Takahashi, K., Ueda, R., et al. (2007). A functional genomics strategy reveals clockwork orange as a transcriptional regulator in the Drosophila circadian clock. Genes Dev. *21*, 1687–1700. https://doi.org/10.1101/gad.1552207.

20. Richier, B., Michard-Vanhée, C., Lamouroux, A., Papin, C., and Rouyer, F. (2008). The clockwork orange Drosophila protein functions as both an activator and a repressor of clock gene expression. J. Biol. Rhythms *23*, 103–116. https://doi.org/10.1177/0748730407313817.

21. Kadener, S., Stoleru, D., McDonald, M., Nawathean, P., and Rosbash, M. (2007). Clockwork Orange is a transcriptional repressor and a new Drosophila circadian pacemaker component. Genes Dev. *21*, 1675–1686. https://doi.org/10.1101/gad.1552607.

22. Zhou, J., Yu, W., and Hardin, P.E. (2016). CLOCKWORK ORANGE Enhances PERIOD Mediated Rhythms in Transcriptional Repression by Antagonizing E-box Binding by CLOCK-CYCLE. PLoS Genet. *12*, e1006430. https://doi.org/10.1371/journal.pgen.1006430.

23. Honma, S., Kawamoto, T., Takagi, Y., Fujimoto, K., Sato, F., Noshiro, M., Kato, Y., and Honma, K.i. (2002). Dec1 and Dec2 are regulators of the mammalian molecular clock. Nature *419*, 841–844. https://doi.org/10.1038/nature01123.

24. Nakashima, A., Kawamoto, T., Honda, K.K., Ueshima, T., Noshiro, M., Iwata, T., Fujimoto, K., Kubo, H., Honma, S., Yorioka, N., et al. (2008). DEC1 modulates the circadian phase of clock gene expression. Mol. Cell Biol. *28*, 4080–4092. https://doi.org/10.1128/MCB.02168-07.

25. Iizuka, K., and Horikawa, Y. (2008). Regulation of lipogenesis via BHLHB2/DEC1 and ChREBP feedback looping. Biochem. Biophys. Res. Commun. *374*, 95–100. https://doi.org/10.1016/j.bbrc.2008.06.101.

26. Zinke, I., Schütz, C.S., Katzenberger, J.D., Bauer, M., and Pankratz, M.J. (2002). Nutrient control of gene expression in Drosophila: microarray analysis of starvation and sugar-dependent response. EMBO J. *21*, 6162–6173. https://doi.org/10.1093/emboj/cdf600.

27. Bailey, T.L. (2011). DREME: motif discovery in transcription factor ChIP-seq data. Bioinformatics *27*, 1653–1659. https://doi.org/10.1093/bioinformatics/btr261.

28. Nitta, K.R., Jolma, A., Yin, Y., Morgunova, E., Kivioja, T., Akhtar, J., Hens, K., Toivonen, J., Deplancke, B., Furlong, E.E.M., and Taipale, J. (2015). Conservation of transcription factor binding specificities across 600 million years of bilateria evolution. Elife *4*, e04837. https://doi.org/10.7554/eLife.04837.

29. Gupta, S., Stamatoyannopoulos, J.A., Bailey, T.L., and Noble, W.S. (2007). Quantifying similarity between motifs. Genome Biol. *8*, R24. https://doi.org/10.1186/gb-2007-8-2-r24.

30. Kokki, K., Lamichane, N., Nieminen, A.I., Ruhanen, H., Morikka, J., Robciuc, M., Rovenko, B.M., Havula, E., Käkelä, R., and Hietakangas, V. (2021). Metabolic gene regulation by Drosophila GATA transcription factor Grain. PLoS Genet. *17*, e1009855. https://doi.org/10.1371/journal.pgen.1009855.

31. Zeidan, Q., Wang, Z., De Maio, A., and Hart, G.W. (2010). O-GlcNAc cycling enzymes associate with the translational machinery and modify core ribosomal proteins. Mol. Biol. Cell *21*, 1922–1936. https://doi.org/10.1091/mbc.E09-11-0941.

32. Hasygar, K., Deniz, O., Liu, Y., Gullmets, J., Hynynen, R., Ruhanen, H., Kokki, K., Käkelä, R., and Hietakangas, V. (2021). Coordinated control of adiposity and growth by anti-anabolic kinase ERK7. EMBO Rep. *22*, e49602. https://doi.org/10.15252/embr.201949602.

33. Minn, A.H., Hafele, C., and Shalev, A. (2005). Thioredoxin-interacting protein is stimulated by glucose through a carbohydrate response element and induces beta-cell apoptosis. Endocrinology *146*, 2397–2405. https://doi.org/10.1210/en.2004-1378.

34. Li, Y., Xie, M., Song, X., Gragen, S., Sachdeva, K., Wan, Y., and Yan, B. (2003). DEC1 negatively regulates the expression of DEC2 through binding to the E-box in the proximal promoter. J. Biol. Chem. *278*, 16899–16907. https://doi.org/10.1074/jbc.M300596200.

35. Rauschmeier, R., Gustafsson, C., Reinhardt, A., A-Gonzalez, N., Tortola, L., Cansever, D., Subramanian, S., Taneja, R., Rossner, M.J., Sieweke, M.H., et al. (2019). Bhlhe40 and Bhlhe41 transcription factors regulate alveolar macrophage self-renewal and identity. EMBO J. *38*, e101233. https://doi.org/10.15252/embj.2018101233.

36. Kreslavsky, T., Vilagos, B., Tagoh, H., Poliakova, D.K., Schwickert, T.A., Wöhner, M., Jaritz, M., Weiss, S., Taneja, R., Rossner, M.J., and Busslinger, M. (2017). Essential role for the transcription factor Bhlhe41 in regulating the development, self-renewal and BCR repertoire of B-1a cells. Nat. Immunol. *18*, 442–455. https://doi.org/10.1038/ni.3694.

37. Lin, C.C., Bradstreet, T.R., Schwarzkopf, E.A., Sim, J., Carrero, J.A., Chou, C., Cook, L.E., Egawa, T., Taneja, R., Murphy, T.L., et al. (2014). Bhlhe40 controls cytokine production by T cells and is essential for pathogenicity in autoimmune neuroinflammation. Nat. Commun. *5*, 3551. https://doi.org/10.1038/ncomms4551.

38. Liu, Z., Li, Z., Mao, K., Zou, J., Wang, Y., Tao, Z., Lin, G., Tian, L., Ji, Y., Wu, X., et al. (2009). Dec2 promotes Th2 cell differentiation by enhancing IL-2R signaling. J. Immunol. *183*, 6320–6329. https://doi.org/10.4049/jimmunol.0900975.

39. Yang, X.O., Angkasekwinai, P., Zhu, J., Peng, J., Liu, Z., Nurieva, R., Liu, X., Chung, Y., Chang, S.H., Sun, B., and Dong, C. (2009). Requirement for the basic helix-loop-helix transcription factor Dec2 in initial TH2 lineage commitment. Nat. Immunol. *10*, 1260–1266. https://doi.org/10.1038/ni.1821.

40. Parisi, F., Riccardo, S., Zola, S., Lora, C., Grifoni, D., Brown, L.M., and Bellosta, P. (2013). dMyc expression in the fat body affects DILP2 release and increases the expression of the fat desaturase Desat1 resulting in organismal growth. Dev. Biol. *379*, 64–75. https://doi.org/10.1016/j.ydbio.2013.04.008.

41. Liu, Z., Selby, C.P., Yang, Y., Lindsey-Boltz, L.A., Cao, X., Eynullazada, K., and Sancar, A. (2020). Circadian regulation of c-MYC in mice. Proc. Natl. Acad. Sci. USA *117*, 21609–21617. https://doi.org/10.1073/pnas.2011225117.

42. Altman, B.J., Hsieh, A.L., Sengupta, A., Krishnanaiah, S.Y., Stine, Z.E., Walton, Z.E., Gouw, A.M., Venkataraman, A., Li, B., Goraksha-Hicks, P., et al. (2015). MYC disrupts the circadian clock and metabolism in cancer cells. Cell Metab. *22*, 1009–1019. https://doi.org/10.1016/j.cmet.2015.09.003.

43. Hsieh, A.L., Zheng, X., Yue, Z., Stine, Z.E., Mancuso, A., Rhoades, S.D., Brooks, R., Weljie, A.M., Eisenman, R.N., Sehgal, A., and Dang, C.V. (2019). Misregulation of Drosophila Myc disrupts circadian behavior and metabolism. Cell Rep. *29*, 1778–1788.e4. https://doi.org/10.1016/j.celrep.2019.10.022.

44. Baker, N.E. (2020). Emerging mechanisms of cell competition. Nat. Rev. Genet. *21*, 683–697. https://doi.org/10.1038/s41576-020-0262-8.

45. Jouffe, C., Cretenet, G., Symul, L., Martin, E., Atger, F., Naef, F., and Gachon, F. (2013). The circadian clock coordinates ribosome biogenesis. PLoS Biol. *11*, e1001455. https://doi.org/10.1371/journal.pbio.1001455.

46. Li, L., Edgar, B.A., and Grewal, S.S. (2010). Nutritional control of gene expression in Drosophila larvae via TOR, Myc and a novel cis-regulatory element. BMC Cell Biol. *11*, 7. https://doi.org/10.1186/1471-2121-11-7.

47. Wu, J., Jiang, X., Li, Y., Zhu, T., Zhang, J., Zhang, Z., Zhang, L., Zhang, Y., Wang, Y., Zou, X., and Liang, B. (2018). PHA-4/FoxA senses nucleolar stress to regulate lipid accumulation in Caenorhabditis elegans. Nat. Commun. *9*, 1195. https://doi.org/10.1038/s41467-018-03531-2.

48. Oie, S., Matsuzaki, K., Yokoyama, W., Tokunaga, S., Waku, T., Han, S.I., Iwasaki, N., Mikogai, A., Yasuzawa-Tanaka, K., Kishimoto, H., et al. (2014). Hepatic rRNA transcription regulates high-fat-diet-induced obesity. Cell Rep. *7*, 807–820. https://doi.org/10.1016/j.celrep.2014.03.038.

49. Ohn, T., Kedersha, N., Hickman, T., Tisdale, S., and Anderson, P. (2008). A functional RNAi screen links O-GlcNAc modification of ribosomal proteins to stress granule and processing body assembly. Nat. Cell Biol. *10*, 1224–1231. https://doi.org/10.1038/ncb1783.

50. Dehennaut, V., Slomianny, M.C., Page, A., Vercoutter-Edouart, A.S., Jessus, C., Michalski, J.C., Vilain, J.P., Bodart, J.F., and Lefebvre, T. (2008).

Identification of structural and functional O-linked N-acetylglucosamine-bearing proteins in Xenopus laevis oocyte. Mol. Cell. Proteomics *7*, 2229–2245. https://doi.org/10.1074/mcp.M700494-MCP200.

51. Qin, W., Lv, P., Fan, X., Quan, B., Zhu, Y., Qin, K., Chen, Y., Wang, C., and Chen, X. (2017). Quantitative time-resolved chemoproteomics reveals that stable O-GlcNAc regulates box C/D snoRNP biogenesis. Proc. Natl. Acad. Sci. USA *114*, E6749–E6758. https://doi.org/10.1073/pnas.1702688114.
52. Pang, Z., Chong, J., Zhou, G., de Lima Morais, D.A., Chang, L., Barrette, M., Gauthier, C., Jacques, P.É., Li, S., and Xia, J. (2021). MetaboAnalyst 5.0: narrowing the gap between raw spectra and functional insights. Nucleic Acids Res. *49*, W388–W396. https://doi.org/10.1093/nar/gkab382.
53. Bailey, T.L., Boden, M., Buske, F.A., Frith, M., Grant, C.E., Clementi, L., Ren, J., Li, W.W., and Noble, W.S. (2009). MEME Suite: tools for motif discovery and searching. Nucleic Acids Res. *37*, W202–W208. https://doi.org/10.1093/nar/gkp335.
54. Li, H., and Durbin, R. (2009). Fast and accurate short read alignment with Burrows–Wheeler transform. Bioinformatics *25*, 1754–1760. https://doi.org/10.1093/bioinformatics/btp324.
55. Li, H., Handsaker, B., Wysoker, A., Fennell, T., Ruan, J., Homer, N., Marth, G., Abecasis, G., and Durbin, R.; 1000 Genome Project Data Processing Subgroup (2009). The Sequence Alignment/Map format and SAMtools. Bioinformatics *25*, 2078–2079. https://doi.org/10.1093/bioinformatics/btp352.
56. Hinrichs, A.S., Karolchik, D., Baertsch, R., Barber, G.P., Bejerano, G., Clawson, H., Diekhans, M., Furey, T.S., Harte, R.A., Hsu, F., et al. (2006). The UCSC genome browser database: update 2006. Nucleic Acids Res. *34*, D590–D598. https://doi.org/10.1093/nar/gkj144.
57. Bolger, A.M., Lohse, M., and Usadel, B. (2014). Trimmomatic: a flexible trimmer for Illumina sequence data. Bioinformatics *30*, 2114–2120. https://doi.org/10.1093/bioinformatics/btu170.
58. Trapnell, C., Pachter, L., and Salzberg, S.L. (2009). TopHat: discovering splice junctions with RNA-Seq. Bioinformatics *25*, 1105–1111. https://doi.org/10.1093/bioinformatics/btp120.
59. Anders, S., Pyl, P.T., and Huber, W. (2014). HTSeq—a Python framework to work with high-throughput sequencing data. Bioinformatics *31*, 166–169. https://doi.org/10.1093/bioinformatics/btu638.
60. Piper, M.D.W., Soultoukis, G.A., Blanc, E., Mesaros, A., Herbert, S.L., Juricic, P., He, X., Atanassov, I., Salmonowicz, H., Yang, M., et al. (2017). Matching dietary amino acid balance to the in silico-translated exome optimizes growth and reproduction without cost to lifespan. Cell Metab. *25*, 610–621. https://doi.org/10.1016/j.cmet.2017.02.005.
61. Heidenreich, S., Witte, N., Weber, P., Goehring, I., Tolkachov, A., von Loeffelholz, C., Döcke, S., Bauer, M., Stockmann, M., Pfeiffer, A.F.H., et al. (2017). Retinol saturase coordinates liver metabolism by regulating ChREBP activity. Nat. Commun. *8*, 384. https://doi.org/10.1038/s41467-017-00430-w.
62. Melvin, R.G., Lamichane, N., Havula, E., Kokki, K., Soeder, C., Jones, C.D., and Hietakangas, V. (2018). Natural variation in sugar tolerance associates with changes in signaling and mitochondrial ribosome biogenesis. Elife *7*, e40841. https://doi.org/10.7554/eLife.40841.
63. Ritchie, M.E., Phipson, B., Wu, D., Hu, Y., Law, C.W., Shi, W., and Smyth, G.K. (2015). limma powers differential expression analyses for RNA-sequencing and microarray studies. Nucleic Acids Res. *43*, e47. https://doi.org/10.1093/nar/gkv007.
64. Kumar, L., and Futschik, M. (2007). Mfuzz: a software package for soft clustering of microarray data. Bioinformation *2*, 5–7. https://doi.org/10.6026/97320630002005.
65. Väremo, L., Nielsen, J., and Nookaew, I. (2013). Enriching the gene set analysis of genome-wide data by incorporating directionality of gene expression and combining statistical hypotheses and methods. Nucleic Acids Res. *41*, 4378–4391. https://doi.org/10.1093/nar/gkt111.
66. Lawrence, M., Huber, W., Pagès, H., Aboyoun, P., Carlson, M., Gentleman, R., Morgan, M.T., and Carey, V.J. (2013). Software for computing and annotating genomic ranges. PLoS Comput. Biol. *9*, e1003118. https://doi.org/10.1371/journal.pcbi.1003118.
67. Schupp, M., Lefterova, M.I., Janke, J., Leitner, K., Cristancho, A.G., Mullican, S.E., Qatanani, M., Szwergold, N., Steger, D.J., Curtin, J.C., et al. (2009). Retinol saturase promotes adipogenesis and is downregulated in obesity. Proc. Natl. Acad. Sci. USA *106*, 1105–1110. https://doi.org/10.1073/pnas.0812065106.
68. Zhang, Y., Liu, T., Meyer, C.A., Eeckhoute, J., Johnson, D.S., Bernstein, B.E., Nusbaum, C., Myers, R.M., Brown, M., Li, W., and Liu, X.S. (2008). Model-based Analysis of ChIP-Seq (MACS). Genome Biol. *9*, R137. https://doi.org/10.1186/gb-2008-9-9-r137.
69. Amemiya, H.M., Kundaje, A., and Boyle, A.P. (2019). The ENCODE blacklist: identification of problematic regions of the genome. Sci. Rep. *9*, 9354. https://doi.org/10.1038/s41598-019-45839-z.
70. Zhu, L.J., Gazin, C., Lawson, N.D., Pagès, H., Lin, S.M., Lapointe, D.S., and Green, M.R. (2010). ChIPpeakAnno: a bioconductor package to annotate ChIP-seq and ChIP-chip data. BMC Bioinformatics *11*, 237. https://doi.org/10.1186/1471-2105-11-237.
71. Gel, B., and Serra, E. (2017). karyoploteR: an R/Bioconductor package to plot customizable genomes displaying arbitrary data. Bioinformatics *33*, 3088–3090. https://doi.org/10.1093/bioinformatics/btx346.
72. Tennessen, J.M., Barry, W.E., Cox, J., and Thummel, C.S. (2014). Methods for studying metabolism in Drosophila. Methods *68*, 105–115. https://doi.org/10.1016/j.ymeth.2014.02.034.

STAR★METHODS

KEY RESOURCES TABLE

REAGENT or RESOURCE	SOURCE	IDENTIFIER
Antibodies		
Rabbit anti-ChREBP	Novus Bio	RRID:AB_10002435
Rabbit anti-BHLHE40	Novus Bio	RRID:AB_10000524
Guinea pig anti-Mlx	Havula et al.[3]	N/A
Chemicals, peptides, and recombinant proteins		
m-Cresol purple	Sigma/Merk	#2303-01-7
Critical commercial assays		
Pierce BCA Protein Assay Kit	ThermoFisher	#23225
Triglyceride Reagent	Sigma Aldrich	#T2449
Free Glycerol Reagent	Sigma Aldrich	#F6428
Bradford reagent	Sigma Aldrich	#B6916
Deposited data		
ChREBP & BHLHE40 ChIPseq (*Mus musculus* liver)	This paper	GSE207199 (sub series GSE207198)
RNAseq of cwo mutant (*D. melanogaster* larvae)	This paper	GSE207199 (sub series GSE207197)
RNAseq of time series (*D. melanogaster* larvae)	This paper	GSE207199 (sub series GSE207196)
Experimental models: Cell lines		
D. melanogaster: Cell line S2	ThermoFisher	R69007
Experimental models: Organisms/strains		
D. melanogaster: cwo mutant: cwo^{B9}	Richier et al.[20]	N/A
D. melanogaster: Trip Val20 control	Bloomington Drosophila Stock Center	BDSC #36303
D. melanogaster: kk control	Bloomington Drosophila Stock Center	BDSC #60100
D. melanogaster: RNAi of cwo	Bloomington Drosophila Stock Center	BDSC #26318
D. melanogaster: RNAi of Gnpnat1	Bloomington Drosophila Stock Center	BDSC #50616
D. melanogaster: FB-Gal4	Bloomington Drosophila Stock Center	Flybase: FBti0013267
D. melanogaster: CG-Gal4	Bloomington Drosophila Stock Center	BDSC #7011
D. melanogaster: Tub-Gal4	Bloomington Drosophila Stock Center	BDSC #5138
D. melanogaster: NP1-Gal4	Bloomington Drosophila Stock Center	Flybase: FBti0159208
D. melanogaster: UAS-myc	Bloomington Drosophila Stock Center	BDSC #9674
D. melanogaster: UAS-cwo	The Zurich ORFeome Project	FlyORF #F000668
D. melanogaster: UAS-cwo	This paper	N/A
D. melanogaster: FB-Gal4; cwo^{B9}	This paper	N/A
D. melanogaster: CG-Gal4; cwo^{B9}	This paper	N/A
D. melanogaster: NP1-Gal4; cwo^{B9}	This paper	N/A
D. melanogaster: UAS-cwo; cwo^{B9}/TM3,GFP	This paper	N/A
D. melanogaster: CWO-GFP	Bloomington Drosophila Stock Center	BDSC #66745
D. melanogaster: myc expression on myc mutant background: $P^{52}12$, w* Myc4 P{αTub84B(FRT.Myc)GAL4.Bb}1/FM7i; P{UAS-GFP.U}3	Bloomington Drosophila Stock Center	BDSC #64766
D. melanogaster: w^{1118}	Bloomington Drosophila Stock Center	BDSC #6326
Mus musculus: Wild Type: B6	The Jackson Laboratory	RRID:IMSR_JAX:000664
Oligonucleotides		
qPCR primers	This paper, Table S4	N/A

(*Continued on next page*)

Continued

REAGENT or RESOURCE	SOURCE	IDENTIFIER
Software and algorithms		
MetaboAnalyst (5.0)	Pang et al.[52]	N/A
R/Bioconductor	R Core Team	https://www.bioconductor.org/
MEME Suite command line tools	Bailey et al.[53]	N/A
BWA (v.0.7.17)	Li and Durbin,[54]	N/A
samtools (v.1.4)	Li et al.[55]	N/A
picard (v2.18.10)	Broad Institute	https://broadinstitute.github.io/picard/index.html
UCSC batch coordinate tool	Hinrichs et al.[56]	N/A
FastQC (v.0.11.2)	Babraham Bioinformatics	https://www.bioinformatics.babraham.ac.uk/projects/fastqc/
Trimmomatic (v.0.33)	Bolger et al.[57]	N/A
Tophat (v.2.1.0)	Trapnell et al.[58]	N/A
HTSeq (v.2.7.6)	Anders et al.[59]	N/A
ProgRes Capture Pro (2.8.8)	Jenoptik	https://www.jenoptik.com/products/cameras-and-imaging-modules/microscope-cameras/software-solutions/image-software-progres-capture-pro
GraphPad (8.4.2)	GraphPad Software	https://www.graphpad.com/
Inkscape (1.2.2)	Inkscape Project	https://inkscape.org
ImageJ	NIH	http://imagej.net
Other		
Fly_aa holidic diet	Piper et al.[60]	N/A
Thermo Q Exactive Focus Quadrupole Orbitrap mass spectrometer coupled with a Thermo Dionex UltiMate 3000 HPLC system	Thermo Fisher Scientific	N/A

RESOURCE AVAILABILITY

Lead contact

Further information and requests for resources and reagents should be directed to and will be fulfilled by the lead contact, Ville Hietakangas (ville.hietakangas@helsinki.fi).

Materials availability

All unique materials generated in this study are available from the lead contact.

Data and code availability

- RNAseq and ChIPseq datasets generated in this study are available in GEO, accession: GSE207199
- All data reported in this paper will be shared by the lead contact upon request.
- This paper does not report original code. Any additional information required to reanalyze the data reported in this paper is available from the lead contact upon request.

EXPERIMENTAL MODEL AND STUDY PARTICIPANT DETAILS

Drosophila lines and husbandry

The *Drosophila* stocks were maintained on a standard lab diet (contents: 6.5% malt (w/v), 3.2% semolina (w/v), 1.8% dry baker's yeast (w/v), 0.6% agar (w/v), 0.7% propionic acid (v/v), 2.5% Nipagine (methyl paraben) (v/v)), at 25°C and a light-dark cycle of each 12 h. All experimental diets contained 0.5% agarose (w/v), 0.7% propionic acid (v/v) and 2.5% Nipagine (v/v)). The yeast diets additionally contained 20%, 10% or 6% dry baker's yeast (w/v), while the high sugar diets contained the aforementioned yeast plus 15% sucrose (w/v).

Fly_aa holidic diet was prepared as previously described with small modifications.[60] Agar concentration was 0.7% for improved larvae feeding and digging, and to reduce autofluorescence due to high agar level in the intestine. Sucrose concentration was slightly

reduced from 1.7% to 1.5%, matching the standard low sugar control diet. Fly_aa diet was supplemented with 0.15% m-Cresol purple (Sigma/Merk#2303-01-7) to detect feeding larvae. A master mix with all the components of the Fly_aa medium except agar, sucrose, cholesterol, and m-Cresol was prepared and stored in aliquots at −20°C. Fully prepared Fly_aa medium was also stored at −20°C in closed tubes for long term storage (>1 month), which had no effects on larval growth and pupariation efficiency (data not shown).

The *cwo*^{B9} mutant was generated in.[20] The myc expressing line on myc mutant background was obtained from Bloomington stock center, BDSC #64766, as well as the CWO-GFP line (BDSC #66745), and the *w*^{1118} stock (BDSC #6326). RNAi and Gal4-driver lines were obtained from Bloomington stock center, unless marked otherwise: Trip Val20 control BDSC #36303, kk control BDSC #60100, *cwo* BDSC #26318; *Gnpnat1* BDSC #50616, FB-Gal4 FLYB:FBti0013267, CG-Gal4 BDSC #7011, Tub-GAL4 BDSC #5138, NP1-Gal4 FLYB:FBti0159208. UAS-*myc* BDSC #9674 and UAS-*cwo* FlyORF #F000668 were obtained from The Zurich ORFeome Project. The following recombinant lines were generated in-house: FB-Gal4; *cwo*^{B9}, CG-Gal4; *cwo*^{B9}, NP1-Gal4; *cwo*^{B9}.

To generate UAS-*cwo*, *cwo*^{B9} flies, full-length cwo cDNA was PCR amplified and cloned into a pUAST vector using Not1 and Kpn1 restriction sites. Transgenic UAS-*cwo* flies were obtained from Genetivision, where the construct was injected into the attP2 site (chromosome 3). In-house, the transgenic line was recombined with the *cwo*^{B9} line to obtain UAS-*cwo*, *cwo*^{B9}. Controls containing the UAS-*cwo* element, but not the *cwo*^{B9} mutation and *vice versa*, were generated in the same recombination scheme.

Mouse hepatocyte culture and treatments

Primary hepatocyte isolation from mice and siRNA-mediated knockdowns were performed as previously described.[61] In short, livers of anesthetized male WT mice were perfused with digestion buffer containing 5000 units of collagenase (Worthington). After filtration and separation by Percoll gradient centrifugation (GE Healthcare), cells were seeded on 12-well plates in Dulbecco's modified Eagle's medium (DMEM) without pyruvate containing 25 mM glucose, 10% fetal bovine serum (FBS), and 1% penicillin/streptomycin. For glucose sensing experiments, cells were cultured for 48 h in glucose free DMEM, 10% FBS, and 1% penicillin/streptomycin followed by 8 h in 0.25 or 25 mM glucose as indicated. For siRNA-mediated knockdown, cell culture media of attached hepatocytes was replaced by 500 μL of DMEM without supplements, and cells transfected with 1 nmol of siRNA (Eurogentec) and 4 μL of Lipofectamine 2000 (Thermo Fisher) per 12-well overnight. Adenoviral overexpression was performed by incubation of hepatocytes with equal titers of Ad5-CMV-GFP or Ad5-CMV-mBHLHE40 (Vector Biolabs) overnight. The next morning, cells were washed with PBS, supplemented with DMEM and supplements, and harvested at indicated times.

METHOD DETAILS

Analysis of pupariation and growth

For the RNAi and overexpression experiments, virgin females of the respective driver line were crossed with males from the RNAi or UAS line, respectively. Egg laying occurred for 24 h on apple juice plates (33.33% apple juice (v/v), 1.75% agar (w/v), 2.5% sugar (w/v), 2.0% Nipagin (v/v)), supplemented with dry yeast, at 25°C. After additional 24 h, 30 1st instar larvae were collected to vials containing yeast or high sucrose diet, respectively, and kept at 25°C. Pupariation was scored every 24 h, and eclosion at the end of the observation period. To determine the growth phenotype of *cwo*^{B9} mutants, flies of the *w*^{1118} and *cwo*^{B9} genotypes were allowed to lay eggs onto apple juice plates, supplemented with dry yeast, and for 24 h at 25°C. First instar larvae were carefully staged, i.e. only animals of the same physical size indicating the same developmental stage, and collected to vials with LSD and HSD, respectively, and maintained at 25°C until pupariation. Pupal volume was determined by measuring the length and the width of 30–50 pupae per genotype and diet using ProgRes Capture Pro 2.8.8. software (Jenoptik), and calculating the volume using the following formula: $4/3\ p(L/2)\ (W/2)^2$ (L, length; W, width).

To analyze pupariation curve data, we calculated a pupariation index that incorporates both development time and the number of individuals that complete the larval stage.[62] Specifically, pupariation index is equal to the maximum of the pupation rate function (pupae/hAEL) over the period of observation. Pupariation index was analyzed using ANOVA with main effects of genotype, diet, and their interaction using JMP software (SAS Institute).

RNAseq and related data analysis

Crosses to obtain the required genotypes for the RNAseq experiments were placed into separate egg laying chambers with apple juice plates, supplemented with dry yeast, and kept at 25°C for 24 h. Carefully staged 1st instar larvae, i.e. only animals of the same physical size indicating the same developmental stage, were subsequently collected to plates with LSD at a controlled density and kept at 25°C. 48 h after egg laying early 2nd instar larvae were transferred to plates containing either LSD (10% yeast) or HSD (10% yeast+15% sucrose) containing 2% blue food dye to differentiate between feeding and non-feeding larvae. For the time course RNAseq, 10 feeding larvae were collected and snap-frozen in liquid nitrogen after 4, 8, and 16 h of high sugar exposure, respectively. For the *cwo*^{B9} RNAseq, 10 feeding larvae per sample were collected and snap-frozen after 8 h of high sugar exposure. The larvae were homogenized in lysis buffer and total RNA was extracted using the Nucleospin RNA II kit (Macherey-Nagel #740955.250) in accordance with the manufacturer's instructions. RNAseq, and sample preparation was performed by the DNA Genomics and Sequencing core facility at the University of Helsinki, Finland, as follows: cDNA libraries were prepared from rRNA depleted samples

using the TruSeq Stranded mRNA kit (Illumina). RNAseq (75 bp single end reads; reverse) was run on 2 technical replicates per sample with an average depth of 30 million reads per sample on the Illumina NextSeq500 using the 75bp cycle kit (Illumina).

Raw sequencing data for all RNA-seq datasets was assessed with FastQC (v.0.11.2) (https://www.bioinformatics.babraham.ac.uk/projects/fastqc/). Trimmomatic (v.0.33)[57] was used for read trimming. The reads were required to be minimum of 36 bases long and scanned with 4-base sliding window with minimum quality score of 15 per base and 20 in both strands. Mapping to genomes (*D. melanogaster*: Flybase R6.10; *Mus musculus*: NCBI GRCm38) was assessed with Tophat (v.2.1.0).[58] HTSeq (v.2.7.6)[59] was used for strand-specific quantification of genes and reads below quality score 10 discarded. The differential expression analysis was performed with R/Bioconductor package limma.[63] Genes above CPM (counts per million) > 1 in at least 2/3 or 3/4 replicates in at least one condition were kept. The Benjamini-Hochberg correction was used for adjusting p values [43]. After careful examination, some of the samples were discarded as outliers (sugar dataset: WT_HSD_4_2, WT_HSD_8_1).

Previously published RNAseq data on control larvae fed (standard lab food) vs. starved (PBS +0.5% agarose food) was downloaded and processed as described earlier from GEO repository (GSE123901).

Temporal clustering of gene expression

Fuzzy clustering was performed with R/Bioconductor MFuzz package[64] for differentially expressed genes in sugar dataset (adj.p.val<0.05 in any comparison, LFC<−0.5/LFC>0.5). Means of log2CPM values were used for clustering. After multiple rounds of testing, 14 clusters were defined to be found. The resulting clusters were divided into ‘‘upregulated’’ and ‘‘downregulated’’ based on the directionality of the temporal expression (log2CPM).

Gene set enrichment

Gene set enrichment was performed with R/Bioconductor piano package.[65] GSA with GSEA’s algorithm was used as enrichment method with 1000 permutations. The enrichment was performed for manually downloaded databases for KEGG (https://www.genome.jp/kegg/), Reactome (https://reactome.org/), Wikipathways (https://www.wikipathways.org/index.php/WikiPathways) and GO (http://geneontology.org/). For *cwo* dataset, the enrichment was performed from all the expressed genes. For clusters, the enrichment was performed for each time point for each cluster separately. The results of these enrichments were combined per cluster by taking the minimum adjusted P.value of each significant pathway.

Prediction of candidate TF regulators

DREME[27] was used for *de novo* motif discovery for genes in each cluster. TOMTOM[29] was used for motif comparison and identification with the database from Nitta et al.[28] in addition to *Drosophila* TF motif databases provided by the MEME Suite.[53] The Markov background model was created for each cluster by using MEME tools, respectively. FASTA sequences of +/− 1 kB up-/downstream of TSS’s for genes interest were fetched from *D. melanogaster* (v. Flybase R6.10) by using GenomicFeatures[66] package in R/Bioconductor.

ChIP and related data analysis

ChIP was performed as described previously.[67] In short, small pieces of frozen liver tissue from *ad libitum*-fed male mice (Wildtype: B6 obtained from the Jackson Laboratory (RRID:IMSR_JAX:000664) used for this and all other mouse experiments) were pulverized in liquid nitrogen and underwent cross-linking in 1% formaldehyde for 15 min, followed by quenching with 1/20 volume of 2.5 M glycine solution, and one wash with 1× PBS. Nuclear extracts were prepared by homogenizing in 20 mM HEPES, 0.25 M sucrose, 3 mM $MgCl_2$, 0.2% NP-40, 3 mM β-mercaptoethanol; complete protease inhibitor tablet (Roche). Chromatin fragmentation was performed by sonication in 50 mM HEPES, 1% SDS, and 10 mM EDTA, using a Bioruptor (Diagenode) for 20 cycles of 30 s at the highest level. Proteins were immunoprecipitated in 50 mM HEPES/NaOH at pH 7.5, 155 mM NaCl, 1.1% Triton X-100, 0.11% Na-deoxycholate, and complete protease inhibitor tablet, using anti-ChREBP (Novus Bio NB400-135) or anti-BHLHE40 (Novus Bio NB100-1800) antibodies. Antibodies were precipitated with a 33% slurry of precleaned protein A Sepharose beads in 0.5% BSA/PBS for 2 h. Crosslinking was reversed overnight at 65°C and DNA isolated using phenol/chloroform/isoamyl alcohol. ChIPseq was performed on DNA of 2 individual C57Bl/6 mice, released from the respective antibody (2 x BHLHE40, 2 x ChREBP, and 2x input control) with an average depth of 20 million reads per sample, 75 bp single end reads at the DNA Genomics and Sequencing core facility at the University of Helsinki, Finland. The samples were run on the Illumina NextSeq500 using the 75bp cycle kit (Illumina).

Raw ChIPseq data for *D.melanogaster* CWO (ENCSR900TNL) and MYC (ENCSR999ZCR) datasets were obtained from ENCODE portal (https://www.encodeproject.org/). *Mus musculus* data for BHLHE40 and ChREBP were generated in-house, while raw ChIPseq data for BHLHE41 was downloaded from GEO repository (GSE93764, Kreslavsky et al., 2017). Samples were mapped to their genomes (*D. melanogaster*: Flybase R6.10; *Mus musculus*: NCBI GRCm38) with BWA (v.0.7.17).[54] Reads below quality 5 were discarded, and maximum mismatches in seed were set to 2 with first 32 subsequences as seed. Unmapped, non-primary and alignments below mapping quality 30 were discarded along duplicates using samtools (v.1.4)[55] and picard (v2.18.10) (https://broadinstitute.github.io/picard/index.html). Fragment sizes were estimated with R/Bioconductor phantompeaktools (https://github.com/kundajelab/phantompeakqualtools). Peaks below q-value 0.05 were called for primary chromosomes with MACS2 (v.2.1.0).[68] Empirical blacklist for mm10 was obtained from ENCODE.[69] The blacklist for dm3 defined by ENCODE was converted to match dm6 with USCS’s batch coordinate conversion tool.[56] Peaks in all replicates were defined as expressed and annotated to the nearest TSS from middle of the peak using respective genomes (*D. melanogaster*: Flybase R6.10; *Mus musculus*: NCBI

GRCm38) with R/Bioconductor's ChIPpeakAnno package.[70] For visualization, the binding profiles were merged using samtools merge.[55] The peak visualizations were performed using by R/Bioconductor's karyoploteR package.[71]

ChIP-qPCR was performed as described previously.[17] In brief, chromatin immunoprecipitation was performed on *Drosophila* S2C (Thermo Fisher R69007) cells incubated with guinea pig anti-Mlx,[3] or guinea pig pre-immune serum in the presence or absence of 50 mM glucose for 6 h (n = 3). To determine the percentage of input pulled down qPCR was performed encompassing the predicted ChoRE (−1345 bp to −1328 bp upstream of the *cwo* TSS, identified by searching for the motif "CATGCTCGGCTCGCGTG" in the *cwo* genomic region). A two-tailed t test (heteroskedastic) was conducted to test for statistical significance between groups, with a p value below 0.05 considered significant.

Metabolomics

One hundred-twenty 1st instar larvae of the control (w^{1118}) and cwo^{B9} genotypes were collected to plates containing 6% yeast diet and kept at 25°C for 24 h. 60 early 2nd instar larvae were then transferred plates containing 6% yeast diet with or without 15% sucrose, respectively, and maintained at 25°C for 24 h. Subsequently, 20 larvae per sample (4 samples per group, 4 groups) were collected onto MQ/PBS plates to remove residual food from larval bodies, and snap-frozen in liquid nitrogen to quench the metabolism. Polar metabolite extraction was achieved by manual homogenization using pellet pestles in cold 80% acetonitrile buffer. Samples were centrifuged 13000 rpm for 10 min at 4°C, and the supernatant was used for further analysis. Sample protein content quantification was performed using the Pierce BCA Protein Assay Kit (Thermo Fisher #23225) following the manufacturer's instructions. LC-MS analysis of polar metabolites was conducted as described previously[30] on the Thermo Q Exactive Focus Quadrupole Orbitrap mass spectrometer coupled with a Thermo Dionex UltiMate 3000 HPLC system (Thermo Fisher). For metabolomics data analysis, the peak intensities were normalized to sample specific protein content. The open-source software MetaboAnalyst 5.0[52] was used to perform quality assessment of the data, including PCA (2D scores plot) and hierarchical clustering dendrogram (distance measure: euclidean, clustering algorithm: ward), as well as to draw a histogram (distance measure: euclidian, clustering algorithm: ward). Two-way ANOVA was used to identify statistically interactions between diet and genotype, and multiple comparisons to test for pairwise differences. A p-value below 0.05 was considered statistically significant.

Triacylglycerol measurements

To determine the triacyglycerol content in control (w^{1118}) and cwo^{B9} larvae reared on either LSD (10% yeast) or HSD (10% yeast+15 %sucrose) until 3rd pre-wandering stage. 10 larvae per sample, 3 samples per group were collected and flash frozen in liquid nitrogen. Larvae were homogenized on ice in 300 μL cold 1xPBS (+0.05% Tween 20), and subsequently heat inactivated at 70°C for 10 min. Triacylglyceride levels were measured using the coupled colorimetric assay (Triglyceride Reagent, #T2449 Sigma Aldrich; Free Glycerol Reagent, #F6428 Sigma Aldrich), as described previously.[72] Protein levels were determined with the Bradford reagent (Sigma Aldrich #B6916) following the manufacturer's instructions and used for sample normalization.

Analysis of food consumption

First instar larvae of control (w^{1118}) and cwo^{B9} larvae were collected onto plates containing LSD (10% yeast) in a controlled density, and maintained at 25°C for 24 h. Larvae were transferred to LSD (10% yeast) or HSD (10% yeast +15% sucrose), respectively, containing 0.1% erioglaucine disodium salt, and maintained at 25°C for 3 h. Ten feeding larvae were collected and snap-frozen in liquid nitrogen. Homogenates were prepared by manual disruption in 1 x PBS and centrifuged. The supernatant (1:1 diluted in 1 x PBS) absorbance was measured at 629 nm. The erioglaucine content per sample was determined using a calibration curve, and the obtained values were normalized to the respective sample protein content.

Quantitative RT-PCR

First instar larvae of Tub-Gal4>cwoOE and Tub-Gal4>FlyORF-control crosses were collected to plates with LSD (10% yeast) with or without 15% sucrose and maintained at 25°C for 24 h. 10 carefully staged early 2nd instar larvae, i.e. only animals of the same physical size indicating the same developmental stage, per sample (4–5 samples per group) were cleaned from residual food on the larval bodies using PBS, and flash-frozen in liquid nitrogen. For larvae expressing endogenous myc on myc deficient background (P{hsFLP}12, w* Myc4 P{αTub84B(FRT.Myc)GAL4.Bb}1/FM7i; P{UAS-GFP.U}3) the following modifications to the same protocol were applied: first instar larvae were collected to LSD (10% yeast +2% blue food dye) or HSD (10% yeast +15% sucrose +2% blue food dye) for 4 h. Larvae were manually homogenized and total RNA extracted using the Nucleospin RNA II kit (Macherey-Nagel #740955.250) according to the manufacturer's instructions. The RNA was then reverse transcribed to cDNA with the SensiFAST cDNA Synthesis kit (Bioline #BIO-65054) according to the manufacturer's instructions. Quantitative RT-PCR was performed using the SensiFAST SYBR No-ROX Kit (Bioline #BIO-98020) according to the manufacturer's instructions on the Light Cycler 480 Real-Time PCR System (Roche) in three technical replicates. Data normalization occurred against *Act42A*, and expression analysis via the ΔΔCT method. The primers used are presented in Table S4.

Microscopic analysis of tissues

CWO-GFP virgins were crossed with w^{1118} males, to avoid possible side effects due to CWO-GFP homozygosity, and allowed to lay eggs for 24 h on apple juice plates supplemented with yeast paste in the center of the plate. Next day, uneaten yeast was removed,

and the eggs were left to hatch for another 24 h. First instar CWO-GFP/+ larvae were transferred on 10% yeast diet at a controlled density of 30 larvae per 5 mL food, in 21 × 72 mm vials. Early 3rd instar larvae were transferred to Fly_aa-mCresol holidic diet for 6 h before sample. The short term holidic diet feeding was performed in 5 mL tubes containing 1 mL Fly_aa for 8–15 larvae per tube. Feeding larvae were partially dissected in saline (0.9% NaCl) to expose visceral tissues and transferred to cold 4% formaldehyde in PBS (Thermo Fisher #28908) for overnight fixation in cold with gentle rocking. Fixed larval tissue was blocked and stained in PBS, 1% BSA, 0.1% Triton X-100. LipidTOX Deep Red (Invitrogen #H34477) was diluted 1:500 and incubated with the samples for 30 min at room temperature. After a 15 min wash samples were incubated in Vectashield with DAPI (Vectashield #H-1200) overnight in cold, followed by full dissection and flat mounting with a custom 60 μm spacer (Scotch Magic Tape 810). Images were acquired with Aurox Clarity LFC HS microscope and processed in ImageJ.

Data analysis and visualization

Data other than RNAseq or ChIPseq were statistically analyzed and plotted using GraphPad Prism (8.4.2, GraphPad Software). Final manuscript figures were assembled using InkScape (1.1.2, The InkScape Project).

QUANTIFICATION AND STATISTICAL ANALYSIS

Statistical details can be found in the relevant methods section and figure legends.